Table 2. The 25 PI3K pathway inhibitors used in this study and their profiles and structures (15–18) (Cont'd)

Akt inhibitors					
Akt inhibitor X (3.6×10^{-6} mol/L) Preclinical	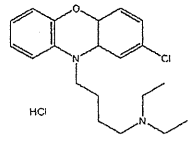	Akt inhibitor XI (1.1×10^{-5} mol/L) Preclinical	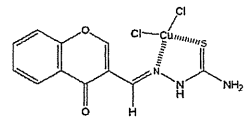		
mTOR inhibitors					
Rapamycin (1.7×10^{-7} mol/L) Allosteric inhibitor of mTORC1 In clinical use	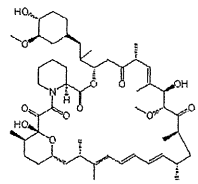	Everolimus (RAD001; 3.6×10^{-8} mol/L) Rapalogue In clinical use	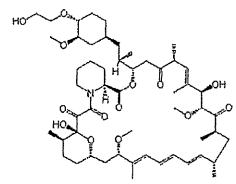	Temsirolimus (CCI779; 2.0×10^{-7} mol/L) Rapalogue In clinical use	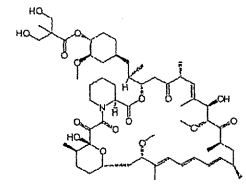

NOTE: Numbers in parentheses are mean GI_{50} values across the JFCR39 cell lines.

mutation would be a biomarker for resistance to these PI3K pathway inhibitors.

Correlation of the efficacy of PI3K pathway inhibitors with protein expression levels of PI3K isoforms, Akt isoforms, and ERBB-family RTKs

We next correlated the expression levels of the above proteins with the efficacy of PI3K pathway inhibitors (Fig. 3A). As a result, we found that expression of p110α had a slight positive correlation with four PI3K inhibitors including IC87114 and LY294002. As for p110β, we found that its high expression correlated with the efficacy of several Akt inhibitors including perifosine. As for Akt isoforms, we found that high expression of Akt2 was associated with the efficacy of five PI3K pathway inhibitors including TGX-221 and LY294002. Correlation analysis between the expression levels of ERBB-family RTKs and the efficacy of PI3K inhibitors revealed no significant correlations with PI3K pathway inhibitors. However, high expression of EGFR correlated with resistance to other classes of anticancer drugs such as navelbine ($r = -0.49$) and mitoxantrone ($r = -0.43$), suggesting that EGFR would confer resistance to these drugs in cancer cells.

Correlation of the efficacy of PI3K pathway inhibitors with phosphorylation levels of the PI3K/Akt and Ras/MAPK pathways

Lastly, we correlated the phosphorylation levels of downstream members of the PI3K pathway with drug efficacy (Fig. 3A). Of note, expression of Akt phosphorylated at S473 had significant correlations with 11 of 25 inhibitors including ZSTK474 ($r = 0.44$; Fig. 3C) and wortmannin ($r = 0.52$). In addition, phosphorylated TSC2 correlated with 7 of 25 inhibitors, including Akt inhibitor IX ($r = 0.41$) and CCI779 ($r = 0.40$). This result suggests that expression levels of Akt phosphorylated at S473 and phosphorylated TSC2 would be predictive markers for these PI3K pathway inhibitors.

Phosphorylated Akt levels and KRAS/BRAF mutation correlated with the *in vivo* efficacy of ZSTK474

We have thus far studied correlations between the status of pathway members and the efficacy of PI3K inhibitors *in vitro*. The most prominent associations were that phosphorylated Akt correlated with the efficacy whereas *KRAS/BRAF* mutation correlated with the inefficacy of PI3K inhibitors including ZSTK474. To test these correlations *in vivo*, we inoculated 24 transplantable cell lines of JFCR39 and examined the antitumor effect of ZSTK474 (Supplementary Fig. S4). We first confirmed that the *in vitro* efficacy pattern across the 24 cell lines significantly correlated with the *in vivo* efficacy pattern (200 mg/kg; $P = 0.02$), suggesting that the *in vivo* efficacy of ZSTK474 reflected its *in vitro* efficacy (Supplementary Fig. S5). Based on these data, we examined the involvement of phosphorylated Akt and *KRAS/BRAF* mutation in the efficacy of ZSTK474 *in vivo* (Fig. 4). The Student *t* test revealed that cell lines having a hotspot mutation in either *KRAS* (G12, G13, and Q61) or *BRAF* (V600) exhibited inefficacy of ZSTK474 ($P = 0.04$; Fig. 4B). Cell lines with PTEN loss such as PC-3 and BSY-1 exhibited susceptibility to ZSTK474, but the difference was not statistically significant across the 24 cell lines. On the other hand, expression levels of phosphorylated Akt in the xenografted tumors significantly correlated with susceptibility to ZSTK474 (Fig. 4C). These results suggest that phosphorylated Akt and *KRAS/BRAF* hotspot mutation could be used as a biomarker for predicting the efficacy of PI3K inhibitors in the clinic.

Discussion

In this study, taking advantage of the JFCR39 cell line panel, we examined the drug efficacy of PI3K pathway inhibitors as well as the status of PI3K and Ras pathway members, and combined them to develop an integrated database. This

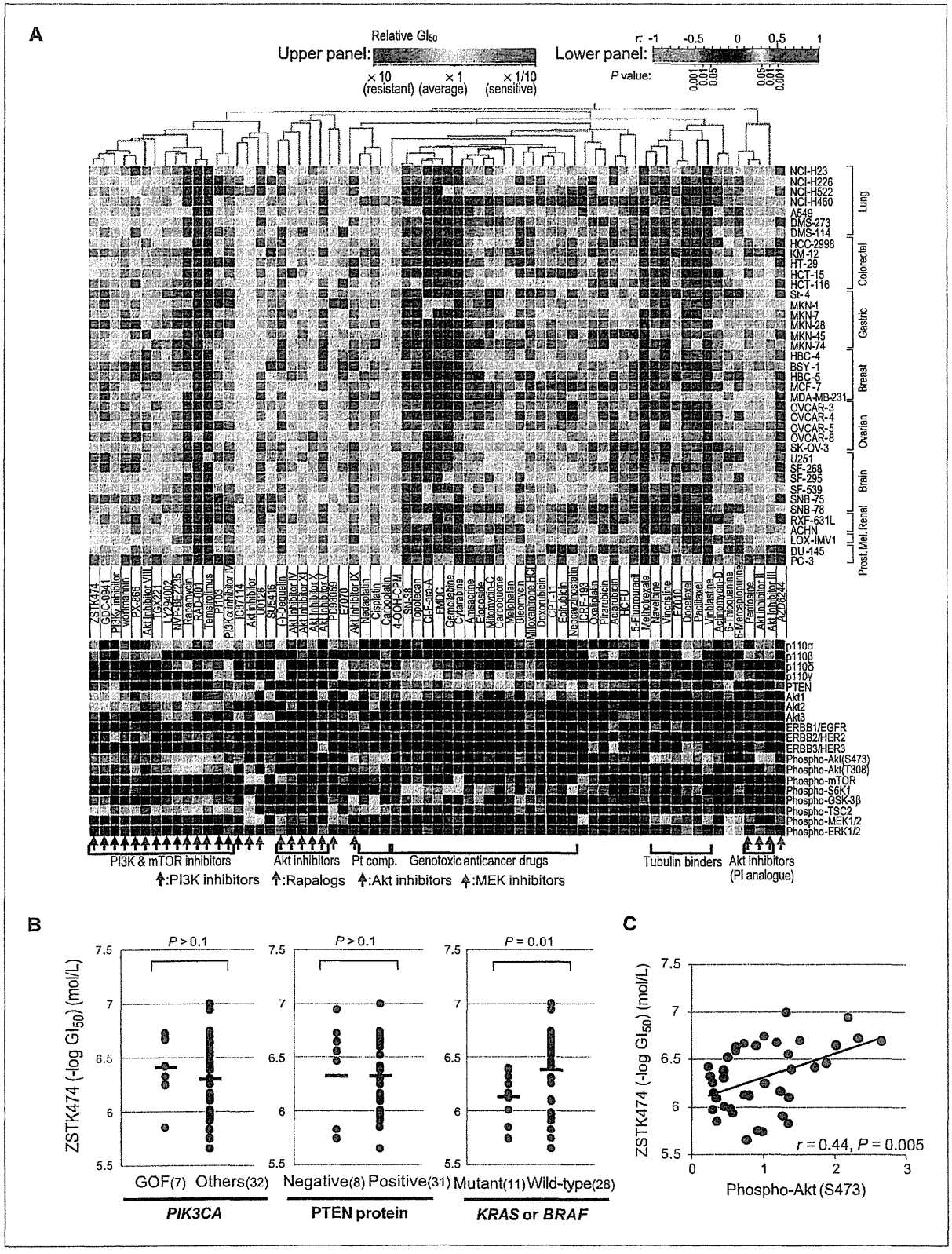
A
Relative GI50
Upper panel:
×10 (resistant)
×1 (average)
×1/10 (sensitive)
Lower panel:
r: -1 -0.5 0 0.5 1
P value:
0.001 0.01 0.05
0.05 0.01 0.001
NCI-H23
NCI-H226
NCI-H522
NCI-H460
A549
DMS-273
DMS-114
HCC-2998
KM-12
HT-29
HCT-15
HCT-116
SW-620
MKN-1
MKN-7
MKN-28
MKN-45
MKN-74
HBC-4
BSY-1
HBC-5
MCF-7
MDA-MB-231
OVCAR-3
OVCAR-4
OVCAR-5
OVCAR-8
SK-OV-3
U251
SF-268
SF-295
SF-539
SNB-75
SNB-78
RXF-631L
ACHN
LOX-IMVI
DU-145
PC-3
Lung
Colorectal
Gastric
Breast
Ovarian
Brain
Renal
Prost.
Mel.
ZSTK474
GDC-0941
PI-103
wortmannin
PX-866
Akt inhibitor VIII
LY294002
NVP-BEZ235
Rapamycin
RAD-001
Temsirolimus
PI103
PI3Kα inhibitor IV
IC87114
Akt inhibitor
U0126
SU5416
(-)-Deguelin
Akt inhibitor IX
Akt inhibitor XI
Akt inhibitor X
Akt inhibitor V
PD98059
E7070
Akt inhibitor IX
Nedaplatin
Cisplatin
Carboplatin
4-OOH-CPM
SN-38
Topotecan
CEP-ara-A
FMDC
Gemcitabine
Cytarabine
Amsacrine
Etoposide
Mitoxantrone
Vinorelbine
Bleomycin
Mitoxantrone HCl
Doxorubicin
CPT-11
Epirubicin
Neocarzinostatin
CRF-193
Oxaliplatin
Pirarubicin
Aclarubicin
HCPU
5-Fluorouracil
Melphalan
Navelbine
Vinorelbine
Estramustine
Docetaxel
Paclitaxel
Vindesine
Actinomycin D
6-Thioguanine
6-Mercaptopurine
Pemetrexed
Akt inhibitor II
Akt inhibitor III
AZD6244
p110α
p110β
p110δ
p110γ
PTEN
Akt1
Akt2
Akt3
ERBB1/EGFR
ERBB2/HER2
ERBB3/HER3
Phospho-Akt(S473)
Phospho-Akt(T308)
Phospho-mTOR
Phospho-S6K1
Phospho-GSK-3β
Phospho-TSC2
Phospho-MEK1/2
Phospho-ERK1/2
PI3K & mTOR inhibitors
Akt inhibitors
Pt comp.
Genotoxic anticancer drugs
Tubulin binders
Akt inhibitors (PI analogue)
:PI3K inhibitors
:Rapalogs
:Akt inhibitors
:MEK inhibitors
B
P > 0.1
P > 0.1
P = 0.01
ZSTK474 (-log GI50) (mol/L)
7.5
7
6.5
6
5.5
GOF(7) Others(32)
Negative(8) Positive(31)
Mutant(11) Wild-type(28)
PIK3CA
PTEN protein
KRAS or BRAF
C
ZSTK474 (-log GI50) (mol/L)
r = 0.44, P = 0.005
0 1 2 3
Phospho-Akt (S473)

database, designated as JFCR39-DB, enabled us to evaluate correlations between the status of pathway members and drug efficacy, as well as correlations among pathway members and among inhibitors *in silico*. First, comparison of the status of pathway members revealed that PTEN loss significantly correlated with upregulated phosphorylation levels of PI3K downstream members and with downregulated phosphorylation levels of Ras downstream members, whereas *KRAS/BRAF* mutation exhibited an opposite tendency. Second, comparison of drug efficacies revealed that most PI3K inhibitors and rapamycins were tightly clustered and were clearly different from other classes of anticancer compounds, suggesting a similarity in the mechanisms of action across these compounds in the cluster. Third, correlation analysis between the status of pathway members and drug efficacy revealed that phosphorylated Akt and *KRAS/BRAF* hotspot mutation correlated with the efficacy and the inefficacy of PI3K inhibitors, respectively. These correlations were confirmed in xenografted human tumors *in vivo*, suggesting that they could serve as predictive biomarkers for PI3K inhibitors.

Correlation analysis among the pathway members revealed that PTEN loss significantly correlated with the phosphorylation levels of Akt, GSK-3β, and TSC2, but *PIK3CA* mutation did not exhibit such correlations, suggesting that PTEN loss was directly connected with activation of these downstream pathway members. Similar results were recently shown by Vasudevan and colleagues using NCI60 cell lines (34) and by Stemke-Hale and colleagues using clinical specimens and cell lines of human breast cancer (35), indicating the significance of PTEN loss in the activation of the PI3K pathway. Furthermore, we showed that PTEN loss was not accompanied by activation of mTOR and S6K1, suggesting the existence of upstream molecule(s) other than Akt that may regulate the activation of mTOR and S6K1. Indeed, mTOR is regulated by energy stress via AMPK and by hypoxia via HIF1α, as well as by growth factor stimulation via PI3K/Akt (13). Interestingly, PTEN loss was strongly associated with inactivation of MAPK pathway components such as MEK1/2 and ERK1/2. Previously, Zimmermann and Moelling reported that phosphorylation of Raf by Akt inhibited activation of the Ras/Raf/MAPK pathway (36), which supports our observation. On the other hand, mutation in either *KRAS* or *BRAF* was strongly correlated with inactivation of PI3K/Akt, rather than activation of the MAPK pathway. This result strongly suggests that gain-of-function mutations of *KRAS* and *BRAF* confer inactivation on Akt and its downstream pathway.

In this study, we performed a mutation analysis of all coding exons of *PIK3CB*, *PIK3CD*, and *PIK3CG* isoforms, which are thought to be rarely mutated in cancer (3). Unexpectedly, we found missense mutations in each isoform that were not registered in the SNP database. Although we could not determine whether they were cancer-specific somatic mutations or derived from germline mutations that have not yet been registered in the SNP database, this is the first report showing that cancer cells harbor missense mutations in these PI3K isoforms. The kinase activities of these mutants compared with their wild-type analogues are under investigation. Cancer cells having these mutations did not exhibit hyperphosphorylation of Akt and its downstream factors, suggesting that they did not activate the canonical PI3K pathway via Akt.

We previously showed that the fingerprints of antitumor compounds across the JFCR39 cell panel can allow evaluation of similarities in the cellular mechanism of action by which drugs exert their antitumor activity (28, 29). Comparison of drug fingerprints revealed that most PI3K inhibitors and rapamycins were tightly clustered and their fingerprints were clearly different from those of other classes of anticancer compounds, suggesting that they act by similar mechanisms, probably by blocking the PI3K/mTOR pathway. Moreover, a fine comparison of the fingerprints of these PI3K pathway inhibitors revealed that ZSTK474 and GDC-0941, both of which are specific class I PI3K inhibitors that do not inhibit other PI3K-related protein kinases including mTOR (15, 37–39), show similar fingerprints ($r = 0.86$). On the other hand, NVP-BEZ235, which is a more potent inhibitor of mTOR than of PI3K (40), exhibited high correlations with the mTOR inhibitor rapamycin ($r = 0.78$), and the correlation was much higher than those with ZSTK474 ($r = 0.67$) and GDC-0941 ($r = 0.46$). Thus, these results suggest that comparison of fingerprints may accurately distinguish the cellular target(s) that determine(s) the susceptibility of cancer cells to these drugs.

Using the integrated PI3K database, we correlated the status of these pathway members with the efficacy of PI3K inhibitors. We first found that either gain-of-function mutation of *PIK3CA* or PTEN loss did not exhibit significant correlation with the efficacy of PI3K inhibitors. Brachmann and colleagues recently reported that NVP-BEZ235 selectively induced apoptosis in *PIK3CA*-mutant breast cancer cells (41). However, in the present study, *PIK3CA*-mutant cell lines did not exhibit hypersensitivity but were susceptible to PI3K inhibitors to a similar extent as those with wild-type *PIK3CA*. Indeed, similar results were obtained in *in vivo* experiments using 24

Figure 3. Fingerprints of 67 compounds including 25 PI3K pathway inhibitors and other conventional anticancer agents and their correlations with the activation status of PI3K pathway members. A, top, the GI_{50} in each cell line was determined and log transformed. The compounds were clustered on the basis of their correlations with other compounds (average-linkage clustered with Pearson correlation metric). Cluster analysis was done by using GeneSpring GX (Agilent Technologies). A yellow point represents the average |log GI_{50}| for each compound across JFCR39. A red point and a blue point represent sensitivity and resistance by 10-fold, respectively. Bottom, a heat map of correlation between the fingerprints of 67 anticancer compounds and those of PI3K pathway members. A red point (high positive Pearson correlation coefficient, $P < 0.001$) indicates that the compound tends to be more effective against cell lines that express more of the protein; a blue point (high negative correlation, $P < 0.001$) indicates the opposite tendency. B, difference in the efficacy of ZSTK474 between cell lines with and without *PIK3CA* gain-of-function mutation, loss of PTEN expression, and *KRAS/BRAF* mutation. C, scatter plots of JFCR39 cell lines showing a significant correlation between phospho-Akt (S473) and the efficacy of ZSTK474.

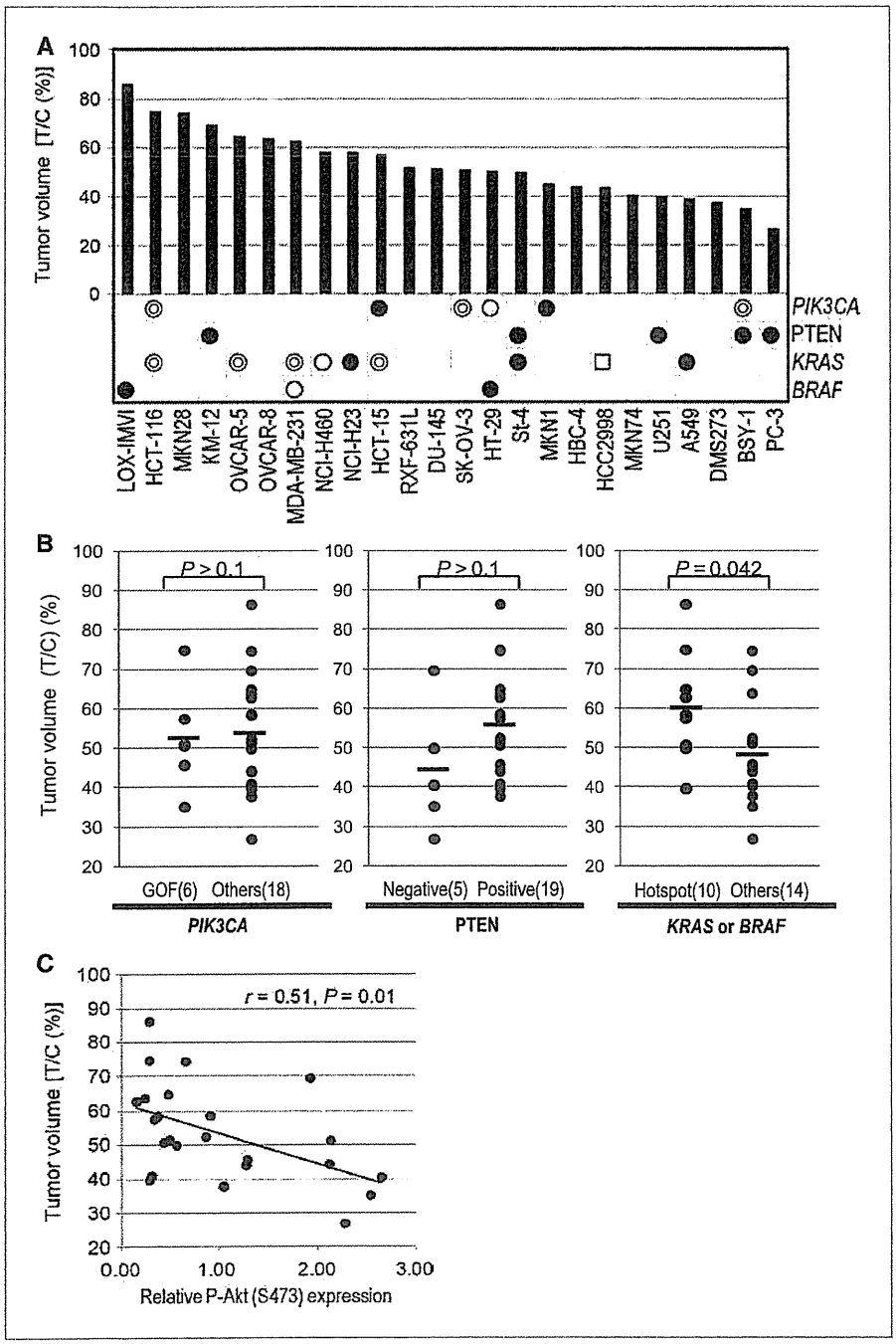

Figure 4. *In vivo* efficacy of ZSTK474 toward human tumors xenografted in nude mice and the activation status of PI3K pathway members. A, 24 transplantable cell lines of JFCR39 were inoculated in nude mice and the *in vivo* efficacy of ZSTK474 (200 mg/kg) was examined (T/C%). The mutation status of *PIK3CA* (closed circle: E545K, double circle: H1047R, open circle: P449T), *PTEN* (closed circle: mutation or deletion without protein expression), *KRAS* (closed circle: G12, double circle: G13, open circle: Q61, open square: A146), and *BRAF* (closed circle: V600E, open circle: G464V) were indicated. B, difference in the *in vivo* efficacy of ZSTK474 between cell lines with and without *PIK3CA* gain-of-function mutation, loss of PTEN expression, and *KRAS/BRAF* hotspot mutation. C, scatter plots of 24 cancer cell lines showing significant correlations between phospho-Akt (S473) expressed in tumor sample and the *in vivo* efficacy of ZSTK474.

transplantable human cancer cell lines xenografted in nude mice (Fig. 4B). We further showed that PI3K inhibitors including ZSTK474 and NVP-BEZ235 inhibit the enzymatic activity of gain-of-function mutant of p110α to an extent comparable to the wild-type (Fig. 1B). These results suggest that such PI3K inhibitors can be used for these cancers. On the other hand, cell lines with mutation in either *KRAS* or *BRAF* exhibited resistance to five PI3K inhibitors including ZSTK474. In *in vivo* studies, we showed that *KRAS/BRAF* mutation exhibited a significant correlation with efficacy of ZSTK474 using 24 xenografted tumors. Similar results were recently reported by Ihle and colleagues by using PX-866 and 13 human tumor xenografts (42) and by Engelman and colleagues using NVP-BEZ235 and a mouse tumor model ectopically expressing a KRAS mutant (23), suggesting the significance of *KRAS/BRAF* mutation in the inefficacy of these PI3K inhibitors.

Of the PI3K pathway downstream members examined in this study, it should be noted that Akt phosphorylated at S473 had significant correlations with 6 of 11 PI3K inhibitors including ZSTK474. Moreover, the correlation between phosphorylated Akt levels and the efficacy of ZSTK474 was confirmed in *in vivo* experiments using 24 human cancer xenografts. This result indicated that the expression level of Akt phosphorylated at S473 could be a candidate biomarker for predicting the efficacy of PI3K inhibitors. The reason why Akt phosphorylated at S473, but not T308, exhibited this correlation is unknown. Phosphorylation of the S473 residue of Akt is known to be catalyzed by the TORC2 complex (whose components include mTOR and rictor) and is required, in addition to T308, for full activation of Akt (43). It is intriguing that the fully activated form of Akt correlated with the efficacy of PI3K inhibitors.

In summary, we constructed an integrated database of PI3K and Ras pathway members and the efficacy of PI3K pathway inhibitors in JFCR39 (JFCR39-DB). *In silico* correlation analysis using JFCR39-DB enabled us to extract two candidates, phospho-Akt and *KRAS/BRAF* mutation, as predictive biomarkers for efficacy of PI3K inhibitors from various pathway members examined. Moreover, we confirmed these correlations by *in vivo* studies using 24 xenografted tumors. The utility of these candidate biomarkers should be validated through clinical studies in future. In addition, JFCR39-DB enabled us to study functional relationships among pathway members and those among drugs. Therefore, JFCR39-DB described here is a useful tool to identify predictive biomarkers, as well as to study the molecular pharmacology of the PI3K pathway in cancer.

Disclosure of Potential Conflicts of Interest

T. Yamori: commercial research grant, Zenyaku Kogyo Co., Ltd. The other authors disclosed no potential conflicts of interest.

Acknowledgments

We thank Yumiko Nishimura and Yoshimi Ohashi for their technical assistance and Zenyaku Kogyo Co. Ltd. for providing us with ZSTK474.

Grant Support

National Institute of Biomedical Innovation, Japan, grant 5-13 (T. Yamori); Grants-in-Aid of the Priority Area "Cancer" from the Ministry of Education, Culture, Sports, Science, and Technology of Japan, nos. 18015049 and 20015048 (T. Yamori); Grants-in-Aid for Scientific Research (B), no. 17390032, and (A), no. 22240092, from the Japan Society for the Promotion of Science (T. Yamori); the Kobayashi Institute for Innovative Cancer Chemotherapy (T. Yamori); and Grants-in-Aid for Young Scientists (B) from the Japan Society for the Promotion of Science, nos. 20790087and 22700929 (S. Dan).

The costs of publication of this article were defrayed in part by the payment of page charges. This article must therefore be hereby marked *advertisement* in accordance with 18 U.S.C. Section 1734 solely to indicate this fact.

Received 11/16/2009; revised 03/25/2010; accepted 04/22/2010; published OnlineFirst 06/08/2010.

References

1. Cantley LC. The phosphoinositide 3-kinase pathway. Science 2002; 296:1655–7.
2. Engelman JA, Luo J, Cantley LC. The evolution of phosphatidylinositol 3-kinases as regulators of growth and metabolism. Nat Rev Genet 2006;7:606–19.
3. Samuels Y, Velculescu VE. Oncogenic mutations of PIK3CA in human cancers. Cell Cycle 2004;3:1221–4.
4. Samuels Y, Wang Z, Bardelli A, et al. High frequency of mutations of the PIK3CA gene in human cancers. Science 2004;304:554.
5. Ma YY, Wei SJ, Lin YC, et al. PIK3CA as an oncogene in cervical cancer. Oncogene 2000;19:2739–44.
6. Shayesteh L, Lu Y, Kuo WL, et al. PIK3CA is implicated as an oncogene in ovarian cancer. Nat Genet 1999;21:99–102.
7. Li J, Yen C, Liaw D, et al. PTEN, a putative protein tyrosine phosphatase gene mutated in human brain, breast, and prostate cancer. Science 1997;275:1943–7.
8. Steck PA, Pershouse MA, Jasser SA, et al. Identification of a candidate tumour suppressor gene, MMAC1, at chromosome 10q23.3 that is mutated in multiple advanced cancers. Nat Genet 1997;15:356–62.
9. Vivanco I, Sawyers CL. The phosphatidylinositol 3-kinase AKT pathway in human cancer. Nat Rev Cancer 2002;2:489–501.
10. Hu L, Zaloudek C, Mills GB, Gray J, Jaffe RB. *In vivo* and *in vitro* ovarian carcinoma growth inhibition by a phosphatidylinositol 3-kinase inhibitor (LY294002). Clin Cancer Res 2000;6:880–6.
11. Ihle NT, Williams R, Chow S, et al. Molecular pharmacology and antitumor activity of PX-866, a novel inhibitor of phosphoinositide-3-kinase signaling. Mol Cancer Ther 2004;3:763–72.
12. Yaguchi S, Fukui Y, Koshimizu I, et al. Antitumor activity of ZSTK474, a new phosphatidylinositol 3-kinase inhibitor. J Natl Cancer Inst 2006;98:545–56.
13. Engelman JA. Targeting PI3K signalling in cancer: opportunities, challenges and limitations. Nat Rev Cancer 2009;9:550–62.
14. Hoeflich KP, O'Brien C, Boyd Z, et al. *In vivo* antitumor activity of MEK and phosphatidylinositol 3-kinase inhibitors in basal-like breast cancer models. Clin Cancer Res 2009;15:4649–64.
15. Kong D, Yamori T. Advances in development of phosphatidylinositol 3-kinase inhibitors. Curr Med Chem 2009;16:2839–54.
16. Ihle NT, Powis G. Take your PIK: phosphatidylinositol 3-kinase inhibitors race through the clinic and toward cancer therapy. Mol Cancer Ther 2009;8:1–9.
17. Knight ZA, Gonzalez B, Feldman ME, et al. A pharmacological map of the PI3-K family defines a role for p110α in insulin signaling. Cell 2006;125:733–47.
18. Liu P, Cheng H, Roberts TM, Zhao JJ. Targeting the phosphoinositide 3-kinase pathway in cancer. Nat Rev Drug Discov 2009;8:627–44.
19. Paez JG, Janne PA, Lee JC, et al. EGFR mutations in lung cancer: correlation with clinical response to gefitinib therapy. Science 2004; 304:1497–500.
20. Lynch TJ, Bell DW, Sordella R, et al. Activating mutations in the epidermal growth factor receptor underlying responsiveness of non-small-cell lung cancer to gefitinib. N Engl J Med 2004;350: 2129–39.
21. Lievre A, Bachet JB, Le Corre D, et al. KRAS mutation status is predictive of response to cetuximab therapy in colorectal cancer. Cancer Res 2006;66:3992–5.
22. Siena S, Sartore-Bianchi A, Di Nicolantonio F, Balfour J, Bardelli A. Biomarkers predicting clinical outcome of epidermal growth factor receptor-targeted therapy in metastatic colorectal cancer. J Natl Cancer Inst 2009;101:1308–24.
23. Engelman JA, Chen L, Tan X, et al. Effective use of PI3K and MEK inhibitors to treat mutant Kras G12D and PIK3CA H1047R murine lung cancers. Nat Med 2008;14:1351–6.
24. Jhawer M, Goel S, Wilson AJ, et al. PIK3CA mutation/PTEN expression status predicts response of colon cancer cells to the epidermal

growth factor receptor inhibitor cetuximab. Cancer Res 2008;68: 1953–61.
25. Sartore-Bianchi A, Martini M, Molinari F, et al. PIK3CA mutations in colorectal cancer are associated with clinical resistance to EGFR-targeted monoclonal antibodies. Cancer Res 2009;69:1851–7.
26. Markman B, Atzori F, Perez-Garcia J, Tabernero J, Baselga J. Status of PI3K inhibition and biomarker development in cancer therapeutics. Ann Oncol 2010;21:683–91.
27. Yamori T, Matsunaga A, Sato S, et al. Potent antitumor activity of MS-247, a novel DNA minor groove binder, evaluated by an *in vitro* and *in vivo* human cancer cell line panel. Cancer Res 1999;59:4042–9.
28. Yamori T. Panel of human cancer cell lines provides valuable database for drug discovery and bioinformatics. Cancer Chemother Pharmacol 2003;52 Suppl 1:S74–9.
29. Shoemaker RH. The NCI60 human tumour cell line anticancer drug screen. Nat Rev Cancer 2006;6:813–23.
30. Paull KD, Shoemaker RH, Hodes L, et al. Display and analysis of patterns of differential activity of drugs against human tumor cell lines: development of mean graph and COMPARE algorithm. J Natl Cancer Inst 1989;81:1088–92.
31. Dan S, Tsunoda T, Kitahara O, et al. An integrated database of chemosensitivity to 55 anticancer drugs and gene expression profiles of 39 human cancer cell lines. Cancer Res 2002;62:1139–47.
32. Sugita H, Dan S, Kong D, Tomida A, Yamori T. A new evaluation method for quantifying PI3K activity by HTRF assay. Biochem Biophys Res Commun 2008;377:941–5.
33. Monks A, Scudiero D, Skehan P, et al. Feasibility of a high-flux anticancer drug screen using a diverse panel of cultured human tumor cell lines. J Natl Cancer Inst 1991;83:757–66.
34. Vasudevan KM, Barbie DA, Davies MA, et al. AKT-independent signaling downstream of oncogenic PIK3CA mutations in human cancer. Cancer Cell 2009;16:21–32.
35. Stemke-Hale K, Gonzalez-Angulo AM, Lluch A, et al. An integrative genomic and proteomic analysis of PIK3CA, PTEN, AKT mutations in breast cancer. Cancer Res 2008;68:6084–91.
36. Zimmermann S, Moelling K. Phosphorylation and regulation of Raf by Akt (protein kinase B). Science 1999;286:1741–4.
37. Kong D, Dan S, Yamazaki K, Yamori T. Inhibition profiles of phosphatidylinositol 3-kinase inhibitors against PI3K superfamily and human cancer cell line panel JFCR39. Eur J Cancer 2010;46:1111–21.
38. Raynaud FI, Eccles SA, Patel S, et al. Biological properties of potent inhibitors of class I phosphatidylinositide 3-kinases: from PI-103 through PI-540, PI-620 to the oral agent GDC-0941. Mol Cancer Ther 2009;8:1725–38.
39. Folkes AJ, Ahmadi K, Alderton WK, et al. The identification of 2-(1*H*-indazol-4-yl)-6-(4-methanesulfonyl-piperazin-1-ylmethyl)-4-morpholin-4-yl-t hieno[3,2-*d*]pyrimidine (GDC-0941) as a potent, selective, orally bioavailable inhibitor of class I PI3 kinase for the treatment of cancer. J Med Chem 2008;51:5522–32.
40. Serra V, Markman B, Scaltriti M, et al. NVP-BEZ235, a dual PI3K/mTOR inhibitor, prevents PI3K signaling and inhibits the growth of cancer cells with activating PI3K mutations. Cancer Res 2008;68: 8022–30.
41. Brachmann SM, Hofmann I, Schnell C, et al. Specific apoptosis induction by the dual PI3K/mTor inhibitor NVP-BEZ235 in HER2 amplified and PIK3CA mutant breast cancer cells. Proc Natl Acad Sci U S A 2009;106:22299–304.
42. Ihle NT, Lemos R, Jr., Wipf P, et al. Mutations in the phosphatidylinositol-3-kinase pathway predict for antitumor activity of the inhibitor PX-866 whereas oncogenic Ras is a dominant predictor for resistance. Cancer Res 2009;69:143–50.
43. Sarbassov DD, Guertin DA, Ali SM, Sabatini DM. Phosphorylation and regulation of Akt/PKB by the rictor-mTOR complex. Science 2005;307:1098–101.

Breast Cancer (2010) 17:118–124
DOI 10.1007/s12282-009-0113-0

ORIGINAL ARTICLE

Clinicopathological analyses of triple negative breast cancer using surveillance data from the Registration Committee of the Japanese Breast Cancer Society

Hirotaka Iwase · Junichi Kurebayashi · Hitoshi Tsuda · Tomohiko Ohta · Masafumi Kurosumi · Kazuaki Miyamoto · Yutaka Yamamoto · Takuji Iwase

Received: 15 January 2009 / Accepted: 10 March 2009 / Published online: 23 May 2009

Abstract
Background Triple negative (TN) breast cancer is defined as a subtype that is negative for estrogen receptor (ER), progesterone receptor (PgR), and human epidermal growth factor receptor 2 (HER2). To clarify the characteristics of TN breast cancer, surveillance data of the Registration Committee of the Japanese Breast Cancer Society were analyzed.
Method Of 14,748 cases registered in 2004, 11,705 (79.4%) were examined for ER, PgR, and HER2. Of these, the most prevalent (53.8%) was a hormone-responsive subtype with ER positive/PgR positive/HER2 negative, followed by TN subtype (15.5%).
Results The proportion of postmenopausal patients was relatively high in the TN subtype. This cancer was diagnosed at a slightly advanced stage and with more cases positive for lymph node metastases than other subtypes. Morphologically, the TN subtype was more frequently classified as solid-tubular carcinoma. Mucinous, tubular, or secretary carcinomas were frequently found in the hormone receptor positive/HER2 negative subtype, while squamous cell carcinoma, spindle cell carcinoma, and metaplastic

H. Iwase · J. Kurebayashi · H. Tsuda · T. Ohta · M. Kurosumi · K. Miyamoto
Member of the Research Group,
Japanese Breast Cancer Society, Tokyo, Japan

H. Iwase (✉) · Y. Yamamoto
Department of Breast and Endocrine Surgery,
Kumamoto University, 1-1-1 Honjo,
Kumamoto 860-8556, Japan
e-mail: hiwase@kumamoto-u.ac.jp

Y. Yamamoto
e-mail: ys-yama@triton.ocn.ne.jp

J. Kurebayashi
Department of Breast and Thyroid Surgery,
Kawasaki Medical University, Okayama, Japan
e-mail: kure@med.kawasaki-m.ac.jp

H. Tsuda
Pathology Section, Clinical Laboratory Division,
National Cancer Center Hospital, Tokyo, Japan
e-mail: hstsuda@ncc.go.jp

T. Ohta
Division of Breast and Endocrine Surgery,
Department of Surgery, St. Marianna University School of Medicine, Kawasaki, Japan
e-mail: to@marianna-u.ac.jp

M. Kurosumi
Department of Pathology, Saitama Prefecture Cancer Center,
Saitama, Japan
e-mail: mkurosumi@cancer-c.pref.saitama.jp

K. Miyamoto
Department of Surgery, National Hospital Organization Kure Medical Center/Chugoku Cancer Center, Kure, Japan
e-mail: miyamotok@kure-nh.go.jp

T. Iwase
Director of the Registration Committee of the Japanese Breast Cancer Society, Tokyo, Japan

T. Iwase
Department of Breast Clinic, Cancer Institute Ariake Hospital,
Tokyo, Japan
e-mail: takiwase@nifty.com

carcinoma with bone/cartilage metaplasia were very frequently found in the TN group. Apocrine carcinoma was also found very frequently in the TN group. Selection of chemotherapy was not based on receptor subtypes, but was determined by the degree of tumor progression.

Conclusions Although TN types are similar to basal-like breast tumor, as determined by gene profiling, their diagnosis needs verification by determination of the level of epidermal growth factor receptor or cytokeratin 5/6 expression. TN type should be examined further for immunohistochemical features and analyzed for prognostic details in this cohort.

Keywords Triple negative tumor · Breast cancer · Surveillance data

Introduction

Triple negative (TN) breast cancer represents a subtype that is negative for the three main prognostic/predictive receptors for breast cancer, namely, estrogen receptor (ER), progesterone receptor (PgR), and HER2 (human epidermal growth factor receptor type 2) [1]. ER and/or PgR positive cancer, which means hormone receptor (HR)-positive cancer, usually responds to endocrine therapy. Cancers scored immunohistochemically as 3+ or 2+ and that are 'fluorescence in situ hybridization' (FISH)-positive are regarded as HER2-positive and are targets for treatment with trastuzumab and other agents aimed at HER2. However, currently no targeted therapeutic agents have been identified specifically for TN breast cancer, and the only option at present is conventional systemic chemotherapy. In this context, it is essential to be familiar with the biological features of TN breast cancer in order to develop the best therapeutic strategy [1–3].

An alternative approach to subtyping breast cancers has been developed by Sørlie et al. [4, 5], who classified breast cancer into four or more intrinsic subtypes on the basis of gene profiling acquired from microarray analyses of a large number of breast cancer tissue specimens. In their classification, the first was called a basal-like subtype; it shared some characteristics with basement membrane cells and had a high proliferative capability [6]. The second was the HER2 (ErbB2) subtype, in which HER2 and related genes were overexpressed and ER-related genes were under expressed. This subtype was also relatively highly proliferative and expected to respond to trastuzumab. The third subtype had normal epithelium (normal-like subtype), but its other significant features have yet to be established. The fourth was called the luminal subtype, which expressed various amounts of ER-related genes that could be further subclassified into luminal A or B. If a connection can be found between the intrinsic subtypes and 'classic' breast cancer subtypes based on receptor status, the correlation is best understood by contrasting the basal-like subtype to TN breast cancer, as the former is positive for cytokeratin 5/6 or epidermal growth factor receptor (EGFR) (HER1).

The basal-like subtype accounts for 15–20% of breast cancers, irrespective of the method of analysis or ethnic group [6]. However, premenopausal African–American patients have a significantly higher incidence of this subtype compared to other patients [7]. It is well known that the pathological and biological characteristics of breast cancer are significantly worse in young African–American patients and that they show a clinically poor prognosis. In contrast, the basal-like subtype is relatively uncommon in breast cancers diagnosed in Japanese women; in 793 breast cancer patients, only 8% were this genetic subtype [8]. A significant overlap has been repeatedly demonstrated between the biological and clinical characteristics of sporadic TN breast cancers and basal-like subtypes, and breast carcinomas arising in BRCA1 mutation carriers [5].

In the receptor subtype determination, there is an ongoing debate on how to determine what to take as the cutoff value for deciding the positive/negative expression levels of hormone receptors. For example, there is no agreement at present on whether 'negative' should be based on: (1) no expression, (2) a score of 0 or 2 on the Allred Score [9], which takes into account the number of positive cells and the intensity of staining for the receptor in question, or (3) the proportion of receptor-positive cells less than 10% [10].

The purpose of this study was to disclose clinicopathological features of TN breast cancer. With the support of the Registration Committee of the Japanese Breast Cancer Society, we analyzed about 11,000 cases registered in 2004 in order to classify them by receptor subtypes based on expression levels of ER/PgR/HER2 and to analyze the clinicopathological characteristics of TN tumors.

Materials and methods

Basic data of patients

Comprehensive data on breast cancer patients diagnosed in Japan in 2004 were registered by the Registration Committee of the Japanese Breast Cancer Society, who reported the final registry data in 2008, although patient outcome data have not been published yet. The registrations were made by 352 institutions and included 14,749 cases. The data collected were: age, clinicopathological features of the tumor including size, presence of lymph node metastases, and receptor status (ER, PgR, and HER2), surgical techniques, and regimens of chemotherapy.

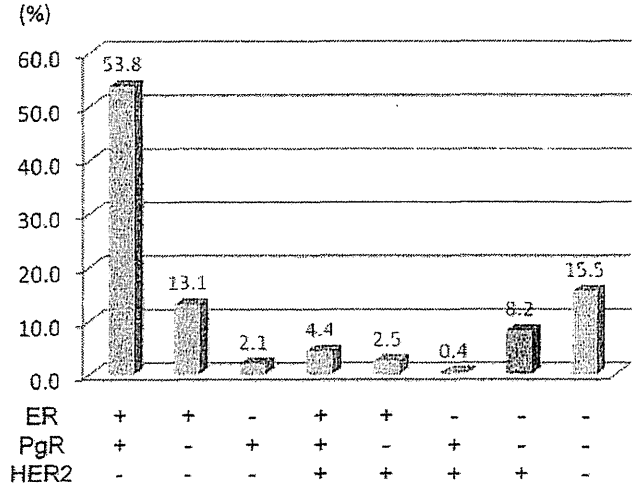

Fig. 1 Breast cancer surveillance data reported by the Japanese Breast Cancer Society

Individual participating institutions determined ER, PgR, and HER2 status by their own in-house method, as well as the other criteria for the registration. In 2004 the status of ER and PgR was being determined by the immunohistochemical (IHC) technique using monoclonal antibodies. Additionally, the cutoff level was mainly adopted to a score of between 2 and 3 on the Allred Score [9], or 10% as a staining proportion [10]. Tumors that were immunohistochemically scored as 3+, or scored 2+ with FISH-positive, were regarded as HER2-positive in a majority of individual participating institutions.

Subanalysis of receptors

Subanalysis was performed by permission of the Registration Committee and the Board of the Japanese Breast Cancer Society. Status of ER, PgR, and Her2 had been determined in 11,705 cases (79.4% of all registered cases), of which 1,819 cases (15.5%) were registered as negative for any one of ER/PgR/HER2. The most prevalent subtype was ER+/PgR+/HER2− (53.8%), followed by TN breast cancer (15.5%) (Fig. 1).

Receptor subtypes were divided according to their ER/PgR/HER2 profiles: the HR+/HER2− subtype was positive for ER and/or PgR and negative for HER2; the HR+/HER2+ subtype was positive for ER and/or PgR and positive for HER2; the HR−/HER2+ subtype was negative for both ER and PgR and positive for HER2; the triple negative (TN) subtype was negative for all three receptors, ER, PgR, and HER2 (Table 1)

Statistical processing

Fischer's exact test was used to compare various prevalence rates among the groups. Unpaired t test was employed to make inter-group comparisons in the number of cases and mean values. A significance level was set at less than 0.01 when multiple comparisons were required between four groups.

Table 1 Receptor subtype and status

Subtype	ER/PgR/HER2 status	
	Receptor profile	ER/PgR/HER2
HR+/HER2−	ER+ and/or PgR+, HER2−	+/+/−, +/−/−, −/+/−
HR+/HER2+	ER+ and/or PgR+, HER2+	+/+/+, +/−/+, −/+/+
HR−/HER2+	ER− and PgR−, HER2+	−/−/+
Triple negative	ER−, PgR− and HER2−	−/−/−

+, Positive; −, negative

Results

Patient backgrounds

The relative proportions of the four cancer subtypes were: HR+/HER2− subtype, 68.7%; HR+/HER2+ subtype, 7.6%; HR−/HER2 subtype, 8.3%; and TN subtype, 15.4%. There was no difference in mean age between the groups. The incidence of bilateral breast cancer was significantly lower in HER2-positive subtypes than in HER2-negative subtypes ($P = 0.040$). The proportion of premenopausal patients was significantly greater in HR-positive groups (i.e., HR+/HER2− and HR+/HER2+ subtypes) than in the HR-negative groups (i.e., HR−/HER2+ or TN subtype) ($P < 0.001$). There were no significant differences between subtypes with respect of family history of breast cancer, height, body weight, or body mass index (BMI) (Table 2). Regarding disease stage, 37.2% of the HR+/HER2− subtype were diagnosed at stage I, indicating relatively early initiation of therapy, whereas the prevalence of stage I at diagnosis in HER2 was only 14.2%, which meant these patients received their first treatment at the slightly advanced stages of II–IV (Fig. 2).

Clinical findings

HR+/HER2− subtype was detected at an earlier stage than the other subtypes, that is, when the tumor was somewhat smaller in diameter, and compared advantageously in the incidence of node metastases especially with the ER−/HER2+ subtype. There was a tendency for the incidence of distant metastases to be higher in the HER2-positive groups (i.e., ER+/HER2+ and ER−/HER2+ subtypes) and for breast-conserving therapy to be less frequently performed in patients with the HR−/HER2+ subtype (Table 2).

Table 2 Patient background and clinicopathological data

	Receptor subtype			
	HR+/HER2−	HR+/HER2+	HER2	TN
Number of patients (%)	8,039 (68.7)	892 (7.6)	977 (8.3)	1,797 (15.4)
Age median (range)	56 (NR–100)	54 (23–93)	56 (22–95)	57.5 (NR–94)
Ratio of bilateral breast cancer (%)	6.6[b]	5.9[a]	4.8[a]	6.2[b]
Incidence of breast cancer family history (%)	8.6	8.4	24.1	28.1
Ratio of premenopausal patients (%)	37.1[c]	38.8[c]	24.1[d]	28.1[d]
Height (cm) mean ± SD	154.3 ± 6.3	154.9 ± 6.1	154.0 ± 6.2	153.8 ± 6.3
Weight (kg) mean ± SD	54.7 ± 9.0	54.5 ± 8.8	53.9 ± 8.6	54.2 ± 9.0
BMI mean ± SD	23.0 ± 3.7	22.7 ± 3.5	22.7 ± 3.3	22.9 ± 3.5
Tumor size (cm) mean ± SD	2.6 ± 2.1[e]	3.2 ± 2.2	3.5 ± 2.6[f]	3.4 ± 2.7
Incidence of positive lymph node involvement (%)	20.6	34.9	38.5	32.2
Incidence of distant metastasis (%)	2.5	5.6	5.6	3.2
Incidence of breast-conserving surgery (%)	53.9	41.3	35.1	45.0

NR no record

[a] HER2 positive versus [b]HER2 negative according to ratio of bilateral breast cancer; $P = 0.040$, Fisher's exact probability test

[c] Hormone receptor-positive group versus [d]hormone receptor-negative group according to the ratio of premenopausal patients; $P < 0.0001$, Fisher's exact probability test

[e] HR+/HER2− subtype versus [f]TN subtype according to tumor size; $P < 0.00001$, standard t test of mean and standard deviation (SD)

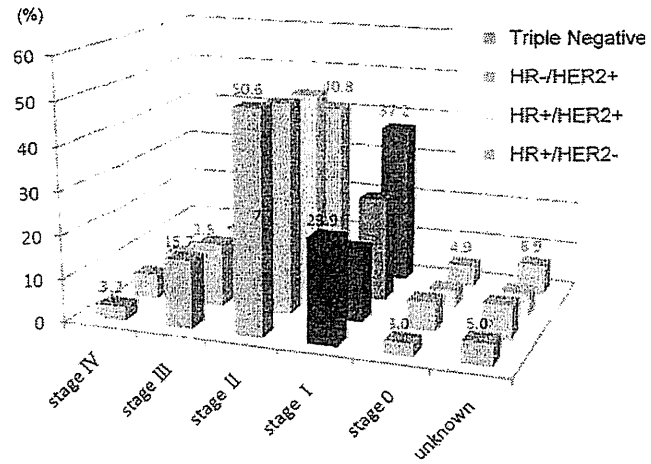

Fig. 2 Stage at diagnosis by receptor subtype

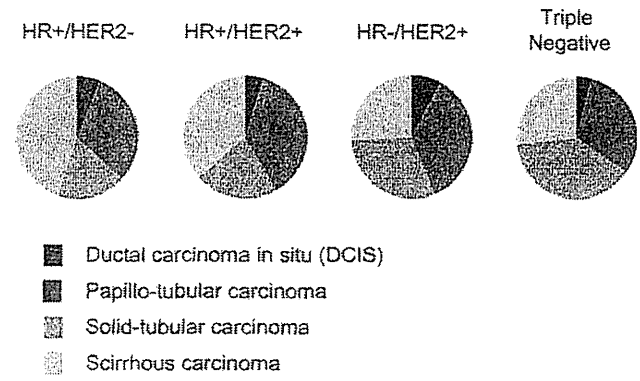

Fig. 3 DCIS and histological subtypes of invasive ductal carcinoma (IDC) by receptor subtype

Pathological findings

From a viewpoint of morphologic classification, whereas scirrhous carcinoma was most frequently found in ER+/HER2− subtype, solid-tubular carcinoma prevailed in TN breast cancer (Fig. 3). As to breast cancers of special types, mucinous carcinoma occurred rarely in the TN group, but was quite frequent among ER+/HER2− subtype patients (Fig. 4a). Invasive lobular carcinoma was found reasonably frequently in the HR+/HER2− type (Fig. 4b). Tubular and secretary carcinomas were mostly found in patients with a HR+/HER2− subtype (Fig. 4c).

Medullary carcinomas were observed frequently in the TN group (Fig. 4d). Squamous cell carcinoma, spindle cell carcinoma, or metaplastic carcinoma with bone/cartilage metaplasia was likewise very common in patients in the TN subtype (Fig. 4e). This group also included the highest percentages of apocrine carcinomas (Fig. 4f).

Selection of chemotherapeutic regimens

Two main chemotherapeutic regimens were administered: (1) anthracycline-containing regimens (ACR), which included: doxorubicin plus cyclophosphamide (AC), epirubicin plus C (EC), C plus A plus 5-fluorouracil (CAF) and CEF, and (2) taxane (paclitaxel or docetaxel)-containing

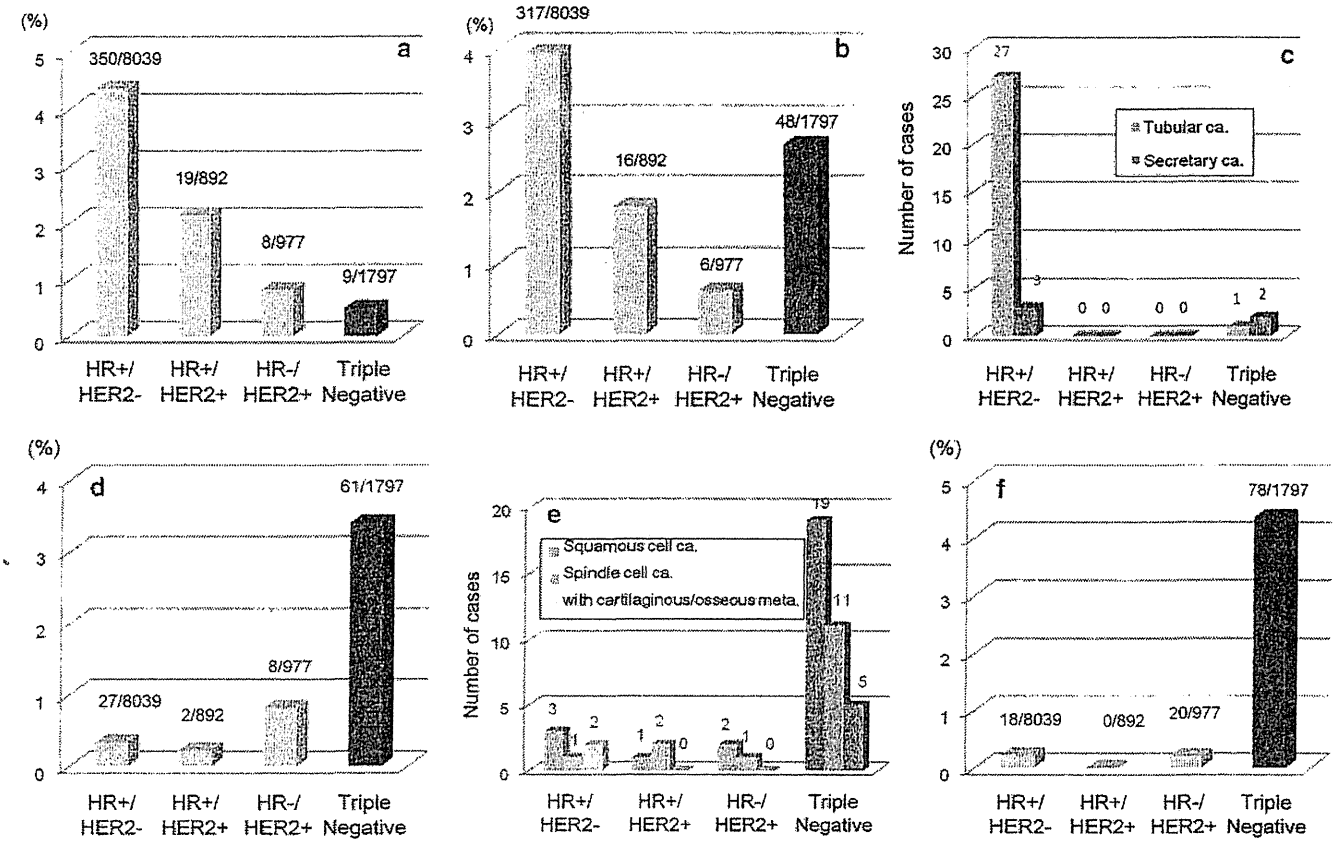

Fig. 4 a Incidence of mucinous carcinoma by receptor subtype. b Incidence of invasive lobular carcinoma by receptor subtype. c Incidence of tubular or secretary carcinomas by receptor subtype. d Incidence of medullary carcinoma by receptor subtype. e Incidence of metastatic carcinoma by receptor subtype. f Incidence of apocrine carcinoma by receptor subtype

Table 3 Chemotherapy according to receptor subtype

	Subtype			
	HR+/HER2−	HR+/HER2+	HR−/HER2+	TN
Number of cases	8,039	892	977	1,797
Node positive cases (%)	20.6	34.9	38.5	32.2
Number of patients treated by chemotherapy	3,913	696	940	1,563
Incidence of patients treated by ACR (%)	28.3	45.0	53.7	49.5
Incidence of patients treated by taxanes (%)	16.9	29.9	36.7	29.2
Incidence of neoadjuvant chemotherapy (%)	25.0	33.9	27.2	25.0

ACR anthracycline-containing regimen

regimens. In one patient there was a possibility that these two main regimens might have been administered concomitantly. ACR was administered to 28.3% of HR+/HER2− subtype tumors and taxane-based regimens to 16.9%. However, the incidence of axillary lymph nodes metastases was 20.6% in this subtype, which was smaller compared to other subtypes. In the other three subtype groups, as shown in Table 3, patients invariably received ACR or taxane regimens. Although the incidence of neoadjuvant chemotherapy was almost identical in each subtype group, the HR+/HER2+ group tended to be treated with this type of chemotherapy a little more frequently (Table 3).

Discussion

Of 14,749 breast cancer cases in Japan in 2004, 11,705 (79.4%) were examined for their ER, PgR, and HER2 status. TN tumors, defined as negative for all three receptors, accounted for 15.5% (1,819 cases). This was the largest collection of data on the prevalence rate of TN

tumors in Japan and was gathered from a large patient sample. Although there were no restrictions placed on the various centers for the methods they used for determining the presence of the receptors, or the criteria employed for their definition, we assumed that most cases had been examined using immunohistochemistry, since this technique for the detection of the receptors was in widespread use in 2004. It is possible that the hormone receptor status of some cases in this current study were incorrectly determined, because the definition criteria had not been established at that time in 2004. Most Japanese institutions regarded 0 or 2 on the Allred score as negative; others used a cutoff value of 10% for the determination of ER/PgR. Currently, the criteria for HER2 positivity are: 3+ with the IHC method, or 2+ with the IHC method and positive with the FISH method. However, in 2004, a tumor was defined as positive for HER2 if the IHC method resulted in 3+ alone, or in 2+ 3+.

Hence, in the present analyses, there were no strict criteria in place for the determination of ER, PgR, or HER2, leaving each institution to apply its own criteria. Now, however, it is considered that standardized analytical methods and definition criteria have been adopted nationwide, so that future analyses will be more reliable. Nevertheless, despite this limitation, we consider that the results of this population study are clinically very significant because of the large number of cases (over 11,000) and participating institutions (over 350).

The basal-like subtype accounts for 15–20% of breast cancers, irrespective of the method of analysis or ethnic group [6]. However, premenopausal African–American patients have a significantly higher incidence of this subtype compared to other patients [7, 11]. It is well known that the pathological and biological characteristics of breast cancer are significantly worse in young African–American patients and that they show a clinically poor prognosis. Therefore, the high incidence of basal-like subtype in young African–American patients correlates with the high histological grade of the tumors and the poor prognosis of the disease in this specific patient subgroup. On the other hand, it has been reported that this basal-like subtype is comparatively rare in Japanese women, with an incidence of only 8% documented in a recent study of 793 breast cancer cases in Japan [8]. We were interested in a possible familial nature of TN tumors, because of suggestions of a link to BRCA1 mutation. In the present study, however, we could not find any evidence of a family history of breast cancer in this subtype or that it affected younger women than other subtypes. This may have been due to the fact that various subtypes of breast cancer are included in the definition of 'TN,' although the basal-like subtype is thought to comprise 40–80% of cases [7, 12].

On the other hand, HR+/HER2− subtype tumors tended to be smaller and the patients freer of lymph node metastases at the time of diagnosis, while the HER2 subtypes were often positive for regional or distant lymph node metastases. This finding indicates the HR+/HER2− subtype tends to be detected at an earlier stage than the HR−/HER2+ subtype, which was characteristically diagnosed at an advanced stage. However, even if these tumors were both detected at an early stage, the difference in outcome would not be affected since HER2-positive tumors progress more rapidly.

Regarding histological subtypes, scirrhous carcinoma and solid-tubular carcinoma tended to be found more frequently in the HR+/HER2− and the TN subtypes, respectively. Although invasive lobular carcinoma was also found in the TN type, its true incidence is unclear as it is rarely difficult to distinguish from scirrhous carcinoma. This TN subgroup also included many cases of medullary and metaplastic carcinomas. Spindle cell and squamous cell carcinomas of the TN tumors showed metaplasia derived from invasive ductal carcinoma and exhibited characteristics of basal-like tumors [12]. However, medullary and apocrine carcinomas, which were included in the metaplastic carcinomas, have a better prognosis than the common type and, among TN breast cancers, should be regarded as different from the more common basal-like breast cancer.

There was no apparent correlation between the choice of chemotherapeutic regimen and tumor receptor subtype, both an anthracycline-containing regimen (ACR) and taxanes were used depending on the degree of progression. Neoadjuvant therapy was used in 27.2 and 25% of HR−/HER2+ and TN tumors, respectively, indicating that in 2004 this therapy was being used in large resectable tumors.

In conclusion, we analyzed data from a large number of breast cancer cases registered by the Japanese Breast Cancer Society in order to characterize and advance our understanding of the TN subtype of breast cancer. The present study demonstrated that it was important to establish standard analytical methods and criteria for detection of ER, PgR, and HER2 and that in particular it was necessary to define TN breast cancer more carefully. In the future, we need to follow up the prognosis and response to chemotherapy in these TN breast cancer cases in an attempt to characterize the subtype in more detail [2]. TN breast cancer simulates basal-like tumor, which has been classified from gene profiles. The basal-like type of TN breast cancer is diagnosed by IHC methods based on the expression of EGFR and cytokeratin 5/6. We are looking into further analyzing the cases from the 2004 registry from the perspectives of immunohistochemistry, prognosis, and use of adjuvant chemotherapy.

Acknowledgment We wish to thank Mr. Naohito Fukui, NPO Japan Clinical Research Support Unit. This work was supported by the research fund from the Japanese Breast Cancer Society.

Conflicts of interest statement. The author and his immediate family members open their conflicts of interest as follows: Employment: none; leadership: none; consultant: none; stock: none; honoraria: H. Iwase, AstraZeneca, Novartis; J. Kurebayashi, AstraZeneca, Takeda; research fund: H. Iwase, AstraZeneca, Taiho, Chugai, Takeda; testimony: none; other: none.

References

1. Bauer KR, Brown M, Cress RD, Parise CA, Caggiano V. Descriptive analysis of estrogen receptor (ER)-negative, progesterone receptor (PR)-negative, and HER2-negative invasive breast cancer, the so-called triple-negative phenotype: a population-based study from the California cancer Registry. Cancer. 2007;109:1721–8.
2. Carey LA, Dees EC, Sawyer L, Gatti L, Moore DT, Collichio F, et al. The triple negative paradox: primary tumor chemosensitivity of breast cancer subtypes. Clin Cancer Res. 2007;13:2329–34.
3. Nishimura R, Arima N. Is triple negative a prognostic factor in breast cancer? Breast Cancer. 2008;15:303–8.
4. Sorlie T, Perou CM, Tibshirani R, Aas T, Geisler S, Johnsen H, et al. Gene expression patterns of breast carcinomas distinguish tumor subclasses with clinical implications. Proc Natl Acad Sci USA. 2001;98:10869–74.
5. Sorlie T, Tibshirani R, Parker J, Hastie T, Marron JS, Nobel A, et al. Repeated observation of breast tumor subtypes in independent gene expression data sets. Proc Natl Acad Sci USA. 2003;100:8418–23.
6. Kobayashi S. Basal-like subtype of breast cancer: a review of its unique characteristics and their clinical significance. Breast Cancer. 2008;15:153–8.
7. Carey LA, Perou CM, Livasy CA, Dressler LG, Cowan D, Conway K, et al. Race, breast cancer subtypes, and survival in the Carolina Breast Cancer Study. JAMA. 2006;295:2492–502.
8. Kurebayashi J, Moriya T, Ishida T, Hirakawa H, Kurosumi M, Akiyama F, et al. The prevalence of intrinsic subtypes and prognosis in breast cancer patients of different races. Breast. 2007;16(Suppl 2):S72–7.
9. Harvey JM, Clark GM, Osborne CK, Allred DC. Estrogen receptor status by immunohistochemistry is superior to the ligand-binding assay for predicting response to adjuvant endocrine therapy in breast cancer. J Clin Oncol. 1999;17:1474–81.
10. Umemura S, Kurosumi M, Moriya T, Oyama T, Arihiro K, Yamashita H, et al. Immunohistochemical Evaluation for hormone receptors in breast cancer: a practically useful evaluation system and handling protocol. Breast cancer. 2006;13:232–5.
11. Millikan RC, Newman B, Tse CK, Moorman PG, Conway K, Dressler LG, et al. Epidemiology of basal-like breast cancer. Breast Cancer Res Treat. 2008;109:123–39.
12. Reis-Filho JS, Milanezi F, Steele D, Savage K, Simpson PT, Nesland JM, et al. Metaplastic breast carcinomas are basal-like tumours. Histopathology. 2006;49:10–21.

Mutation Research 686 (2010) 30–38

Contents lists available at ScienceDirect

Mutation Research/Fundamental and Molecular Mechanisms of Mutagenesis

journal homepage: www.elsevier.com/locate/molmut
Community address: www.elsevier.com/locate/mutres

Complicated biallelic inactivation of *Pten* in radiation-induced mouse thymic lymphomas

Yu Yamaguchi[a,b,1,2], Takashi Takabatake[b,1], Shizuko Kakinuma[b], Yoshiko Amasaki[b], Mayumi Nishimura[b], Tatsuhiko Imaoka[b], Kazumi Yamauchi[b], Yi Shang[b], Tomoko Miyoshi-Imamura[b,c], Hiroyuki Nogawa[a], Yoshiro Kobayashi[d], Yoshiya Shimada[b,*]

[a] *Department of Biology, Graduate School of Science, Chiba University, Yayoicho, Inage-ku, Chiba 263-8522, Japan*
[b] *Experimental Radiobiology for Children's Health Research Group, Research Center for Radiation Protection, National Institute of Radiological Sciences, 4-9-1, Anagawa, Inage-ku, Chiba 263-8555, Japan*
[c] *Genetic Counseling Program, Graduate School of Humanities and Sciences, Ochanomizu University, 2-1-1 Otsuka, Bunkyou-ku, Tokyo 112-8610, Japan*
[d] *Department of Biomolecular Science, Faculty of Science, Toho University, Miyama 2-2-1, Funabashi, Chiba 274-8510, Japan*

ARTICLE INFO

Article history:
Received 29 September 2009
Accepted 29 December 2009
Available online 7 January 2010

Keywords:
Pten
Thymic lymphoma
Epigenetic silencing
Mutation
Deletion
Radiation

ABSTRACT

Inactivation of the phosphatase and tensin homolog gene (*Pten*) occurs via multiple tissue-dependent mechanisms including epigenetic silencing, point mutations, insertions, and deletions. Although frequent loss of heterozygosity around the *Pten* locus and plausible involvement of epigenetic silencing have been reported in radiation-induced thymic lymphomas, the proportion of lymphomas with inactivated *Pten* and the spectrum of causal aberrations have not been extensively characterized. Here, we assessed the mode of *Pten* inactivation by comprehensive analysis of the expression and alteration of *Pten* in 23 radiation-induced thymic lymphomas developed in B6C3F1 mice. We found no evidence for methylation-associated silencing of *Pten*; rather, complex structural abnormalities comprised of missense and nonsense mutations, 1- and 3-bp insertions, and focal deletions were identified in 8 of 23 lymphomas (35%). Sequencing of deletion breakpoints suggested that aberrant V(D)J recombination and microhomology-mediated rearrangement were responsible for the focal deletions. Seven of the 8 lymphomas had biallelic alterations, and 4 of them did not express Pten protein. These *Pten* aberrations coincided with downstream Akt phosphorylation. In conclusion, we demonstrate that *Pten* inactivation is frequently biallelic and is caused by a variety of structural abnormalities (rather than by epigenetic silencing) and is involved in radiation-induced lymphomagenesis.

1. Introduction

The phosphatase and tensin homolog (Pten) is an important lipid phosphatase that antagonizes the phosphatidylinositol-3-kinase (PI3K)/Akt signaling pathway [1,2]. The PI3K/Akt signaling pathway is aberrantly activated in a variety of tumors, often resulting from defects in the *PTEN* gene [3,4]. Once activated, Akt promotes fundamental cellular processes such as cell survival, growth, proliferation, angiogenesis, and cellular metabolism. Pten also plays a crucial role as guardian of genome integrity by maintaining chromosomal stability through physical interaction with centromeres and by controlling DNA repair, both of which are independent of Akt activation [5].

PTEN is mutated in a variety of human carcinomas [6,7], and *PTEN* is the second most frequently mutated gene in human cancers after *TP53* [8,9]. Germline mutations of *PTEN* in humans are responsible for Cowden disease, which is characterized by a high risk for thyroid and breast cancers [10]. In addition to genetic alterations resulting in missense, nonsense or frameshift mutations, epigenetic silencing of *PTEN* has been reported in the pathogenesis of gastric and breast cancers [11,12]. Furthermore, overexpression of *PTEN*-targeting microRNAs correlates with decreased expression of PTEN protein in hepatocellular [13] and ovarian cancers [14]. These reports indicate that there are multiple mechanisms responsible for *PTEN* inactivation.

Interestingly, there are significant differences in the location of mutations in *PTEN* with respect to cancer type. For example, a high proportion of glioblastomas have missense mutations in exon 6, which encodes part of the phosphatase domain of PTEN, whereas few mutations have been found in exons 7 and 8, which encode

* Corresponding author. Tel.: +81 43 206 3200; fax: +81 43 206 4138.
E-mail address: y_shimad@nirsgo.jp (Y. Shimada).
[1] These authors contributed equally to this study.
[2] Present address: Pharmaceutical Research Laboratories, Sanwa Kagaku, Kenkyusho Co., Ltd., 363 Shiosaki, Hokusei-cho, Inabe-shi, Mie 511-0406, Japan.

0027-5107/$ – see front matter © 2010 Elsevier B.V. All rights reserved.
doi:10.1016/j.mrfmmm.2009.12.011

Table 1
Summary of expression and aberrations of Pten in 23 thymic lymphomas, in parallel with the activation of a downstream factor of Akt.

Tumor ID	LOH[a] status	Structural alteretations[b]	Transcriptional changes[b]	Predicted changes[c]	Pten protein	Akt protein[d]
TL5	–	Duplication of exon6 and exon7 509 Ins TGT	Additional faint long product nd	Ins of 103 amino acids 170S→ M and C	A faint larger band Low	Activated
TL14	C3H	Del of exon4 and exon5 9621ns A	Additional faint short product nd	Stop at codon264 Stop at codon333	Absent Absent	Activated
TL8	B6	Homozygous deletion	Absent	–	Absent	Activated
TL11	C3H	Homozygous deletion	Aberant splicing	Stop at codon54	Absent	Activated
TL20	B6	Homozygous deletion	Lack of sequence for exon 1	–	Absent	Activated
TL15	–	862 G→ G/T	nd	Stop codon	Low	Activated
TL19	C3H	158 T→ T/C[e]	nd	53 V→ A	Low	nd
TL21	C3H	364 A→ T	nd	122 I→ F	Low	Activated
TL12	C3H	nd	nd	–	Low	Activated
TL3	–	nd	nd	–	Low	nd
TL6	–	nd	nd	–	Low	nd

[a] Lost allele is shown. (–), retention of heterozygosity.
[b] Ins, insertion; Del, deletion; nd, not detected.
[c] S, serine; M, methionine; C, cysteine; V, valine; A, alanine; I, isoleucine; F, phenylalanine.
[d] "Activated" means that the phosphorylation of Akt protein at Ser473 was detected; nd, not detected.
[e] Sequencing analysis indicates the presence of both mutated and non-mutated sequence, the latter of which may be due to contaminated normal cells.

the C2 domain. In contrast, endometrial carcinomas rarely contain mutations in exon 6; rather, frameshift mutations in exons 7 and 8 are common [6,7]. Deletion of *PTEN* has been identified in 77% of prostate cancer cases, with 25% containing homozygous deletions [15]. Because previous studies have examined only single or limited categories of causal alterations, the overall contribution of each causal *PTEN* alteration remains unclear for many tumor types.

Radiation is a clear etiology for leukemia and lymphoma. Radiation-induced murine thymic lymphomas have been used as a suitable model of human T-cell acute lymphoblastic leukemia (ALL), many of which exhibit *Notch1* and *Ikaros* mutation, *p15* and *p16* alteration, and aberrant activation of Jak-Stat signaling [16–20]. Loss of heterozygosity (LOH) within a broad genomic region of chromosome 19, including the mouse *Pten* locus, has been demonstrated in many thymic lymphomas [21,22]. Although it has been suggested that *Pten* undergoes epigenetic silencing by DNA methylation in radiation-induced murine thymic lymphomas [22], direct evidence has not yet been reported.

To identify the mode of *Pten* inactivation in hematopoietic malignancies, we systematically analyzed the status of *Pten* alleles and Pten expression at the RNA and protein levels in 23 radiation-induced thymic lymphomas developed in B6C3F1 mice; downstream activation of Akt was also analyzed. These analyses revealed that biallelic structural abnormality of *Pten*, but not epigenetic silencing, plays a significant role in radiation-induced lymphomagenesis.

2. Materials and methods

2.1. Tumor induction

The induction of thymic lymphomas was carried out as described [23], with minor modifications. In brief, female B6C3F1 mice were exposed weekly to 2.0 Gy whole-body X-ray radiation for four consecutive weeks starting at four weeks of age. Mice were observed daily until moribund and were then sacrificed under ether anesthesia. All experiments with mice were conducted according to the legal regulations in Japan and were in compliance with the guidelines for the care of laboratory animals of the National Institute of Radiological Sciences.

2.2. LOH analysis

For LOH analysis, genomic DNA was amplified by PCR using the following polymorphic markers: *D19Mit59*, *D19Mit46*, *D19Mit19*, *D19Mit53* and *D19Mit34* (see Supplementary Table 1). To determine LOH at the *Pten* locus, the microsatellite sequence was searched using the UCSC Genome Bioinformatics database (http://genome.ucsc.edu/). A repetitive region within intron 2, which contained fragment length polymorphism between C57BL/6 and C3H/HeJ mice, was identified. PCR products amplified from genomic DNA of C57BL/6 and C3H/HeJ mice that contained this region were sequenced, and the polymorphism was confirmed. The primer sequences and the conditions for each PCR reaction are described in Supplementary Table 1. PCR products were resolved using a capillary electrophoresis system HAD-GT12 Genetic Analyzer (eGene Inc., Irvine, CA, USA) or by 3% NuSieve agarose (3:1) gel electrophoresis (FMC, Rockland, MA, USA).

2.3. RT-PCR analysis

Total RNA was extracted from tumor tissues using the acid guanidinium thiocyanate–phenol-chloroform method [24], and the cDNA was reverse transcribed using 10 μg total RNA, Moloney murine leukemia virus reverse transcriptase (Toyobo Co., Ltd., Osaka, Japan), and random hexamers (Takara Bio) according to the manufacturer's recommendations. The primer sequences and the conditions for each PCR reaction are described in Supplementary Table 1. PCR products were resolved by 2% agarose gel electrophoresis and analyzed using a Luminescent image analyzer LAS-3000 (Fujifilm, Tokyo, Japan). PCR products were directly sequenced using a Big Dye Terminator v3.1 (Applied Biosystems, Foster City, CA, USA) and an ABI PRISM 3100 Genetic Analyzer (Applied Biosystems) or sequenced after TA cloning using a TOPO TA cloning kit (Invitrogen Co., Carlsbad, CA, USA).

2.4. Bisulfite sequencing analysis

Genomic DNA (1.0 μg) was subjected to bisulfite modification using a CpGenome DNA modification kit, No. S7820 (Chemicon, Temecula, CA, USA), according to the manufacturer's instructions. Bisulfite-modified DNA (40 ng/μl) was then subjected to PCR amplification using primers specific for methylated CpG cytosines as described in Supplementary Table 1. PCR products were sequenced after TA cloning.

2.5. Western blot analysis

Thymic lymphoma cells and normal thymocytes were dissolved in cell lysis buffer (Cell Signaling Technology Inc., Danvers, MA, USA) containing phenylmethanesulfonyl fluoride. Proteins were denatured by heating at 100 °C for 5 min in sample buffer containing SDS, and then lysates (20 μg) were separated by 10% SDS-PAGE and transferred to a PVDF membrane (Millipore Co., Billerica, MA, USA). Anti-Pten, anti-Akt, anti-phospho-Akt (Ser473) and anti-beta-actin (Santa Cruz Biotechnology Inc., Santa Cruz, CA, USA) were used as primary antibodies. Horseradish peroxidase-conjugated anti-rabbit (Cell Signaling Technology) or anti-goat (Santa Cruz Biotechnology) IgG was used as secondary antibody. Signals were developed using ECL plus Western Blotting Detection Reagents (GE Healthcare, Little Chalfont, Buckinghamshire, UK) and analyzed using the LAS-3000 luminescent image analyzer (Fujifilm).

2.6. Array-CGH analysis

We designed and used an Agilent 8 × 15k-formatted mouse custom array-CGH microarray (#020410; Agilent Technologies, Santa Clara, CA, USA), which consisted of about 15,000 oligonucleotide probes, including 1499 for the genomic region covering the *Pten* locus on chromosome 19 (about 430 kbp). Fluorescence labeling of DNA, microarray hybridization and post-hybridization washing were carried out according to the manufacturer's protocol (version 5) for genomic DNA analysis using oligonucleotide array-CGH. Scanning was performed using an Agilent microarray scanner (G2565BA). Signal intensities were measured and evaluated using Agilent

Feature Extraction software v9-5-35 and CGH analytics software v3-5-14, respectively. The microarray data reported in this article have been deposited in the Gene Expression Ominibus (GEO) database, www.ncbi.nlm.nih.gov/geo (accession no. GSE17751).

2.7. Quantitative real-time RT-PCR

Quantitative real-time RT-PCR analysis of miR-19a and miR-21 was performed using a TaqMan MicroRNA assay kit (Applied Biosystems) according to manufacturer's recommendations. Quantitative PCR amplification of cDNAs was performed using a Mx3000P real-time PCR system (Stratagene, La Jolla, CA, USA) and TaqMan Universal PCR Master Mix (Applied Biosystems). Data were normalized to the levels of the small nucleolar RNAs 202 and 234. Each reaction was performed in triplicate. Data were analyzed with MxPro software, version 4.10 (Stratagene).

3. Results

3.1. LOH analysis

Mouse *Pten* encodes a protein product predicted to have 403 amino acid residues and is located at 24.5 cM on chromosome 19. We analyzed LOH using five independent microsatellite simple-sequence-length polymorphism makers on chromosome 19. LOH at the *Pten* locus was also examined using a microsatellite marker within intron 2, which distinguished the polymorphism between C57BL/6 and C3H/HeJ mice. LOH around the *Pten* locus was identified in seven lymphomas (TL8, 11, 12, 14, 19, 20 and 21) (Fig. 1). The LOH frequency (30%; 7 of 23 lymphomas) was roughly consistent with previous studies examining radiation-induced thymic lymphomas in various F1 hybrid mouse strains [22,23,25].

3.2. Expression of Pten mRNA and protein

We examined the expression of *Pten* transcripts by reverse transcriptase (RT)-PCR analysis using three sets of primers (Fig. 2). Altered expression of *Pten* mRNA was observed in 5 of 23 lymphomas (TL5, 8, 11, 14 and 20). TL5 had an additional but faint PCR product that was larger than the predicted product when amplified using primers Ex2F and Ex7R. For TL8, RT-PCR products generated using any primer combination were faint or undetectable. LOH at the *Pten* locus in TL8 indicated that one *Pten* allele remained. Thus the absence of *Pten* transcripts suggested the transcriptional silencing at the *Pten* promoter region in the remaining allele. Using the Ex1F-7R primer pair, TL11 generated one RT-PCR product of the predicted length and three longer RT-PCR products; TL14 generated a faint, short RT-PCR product in addition to a product of the predicted length. TL20 generated a faint product when primers Ex1F and Ex7R were used, but a substantial amount of product was generated using either of the remaining two sets of primers, suggesting that a 5′ portion of exon 1 was missing.

3.3. Sequencing of bisulfite-modified DNA

Because our data for TL8 implicated transcriptional silencing of *Pten* (Figs. 1 and 2), we analyzed the DNA methylation pat-

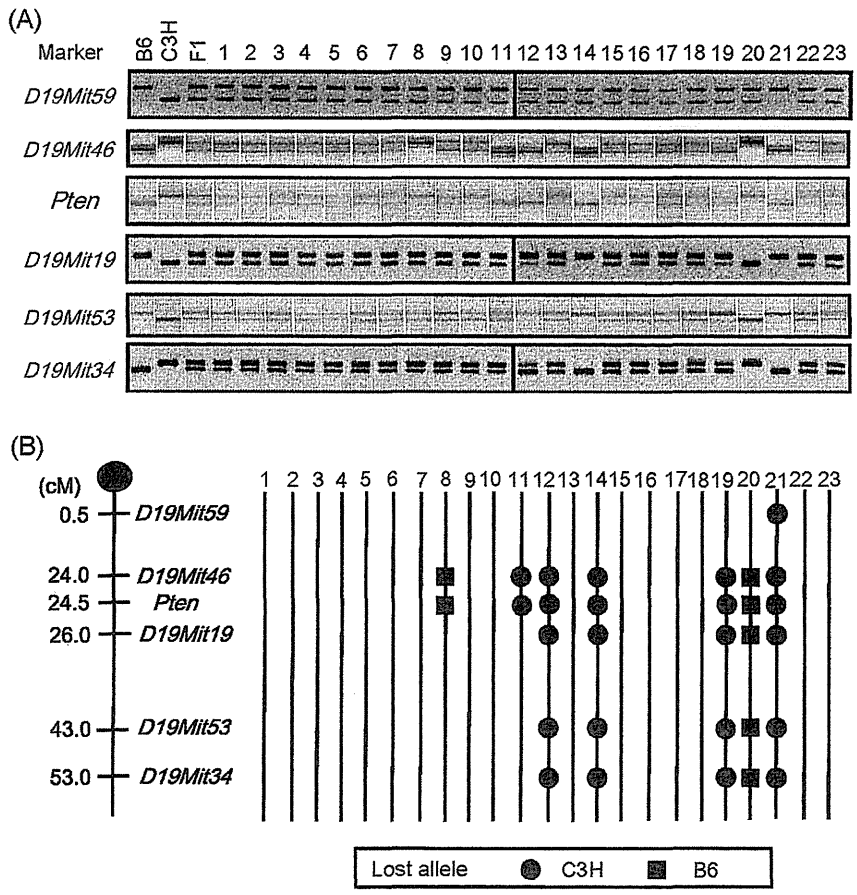

Fig. 1. LOH analysis of chromosome 19 in 23 radiation-induced thymic lymphomas. (A) The first three lanes represent control DNA samples from the maternal C57BL/6 strain (B6), the paternal C3H/HeJ strain (C3H), and the B6C3F1 hybrid (F1), respectively. Numbers above the remaining lanes reflect the tumor identification numbers. PCR amplification of genomic DNA was performed using the indicated polymorphic marker primer pair followed by electrophoretic analysis of amplification products. (B) Schematic diagram of LOH on chromosome 19 in each lymphoma. Lymphoma identification numbers are indicated at top. Polymorphic markers are shown to the right of the chromosome schematic, and marker positions indicating distances (cM) from the centromere are shown at left. The *Pten* marker is located between exons 2 and 3. Absence of a circle or square indicates the retention of heterozygosity.

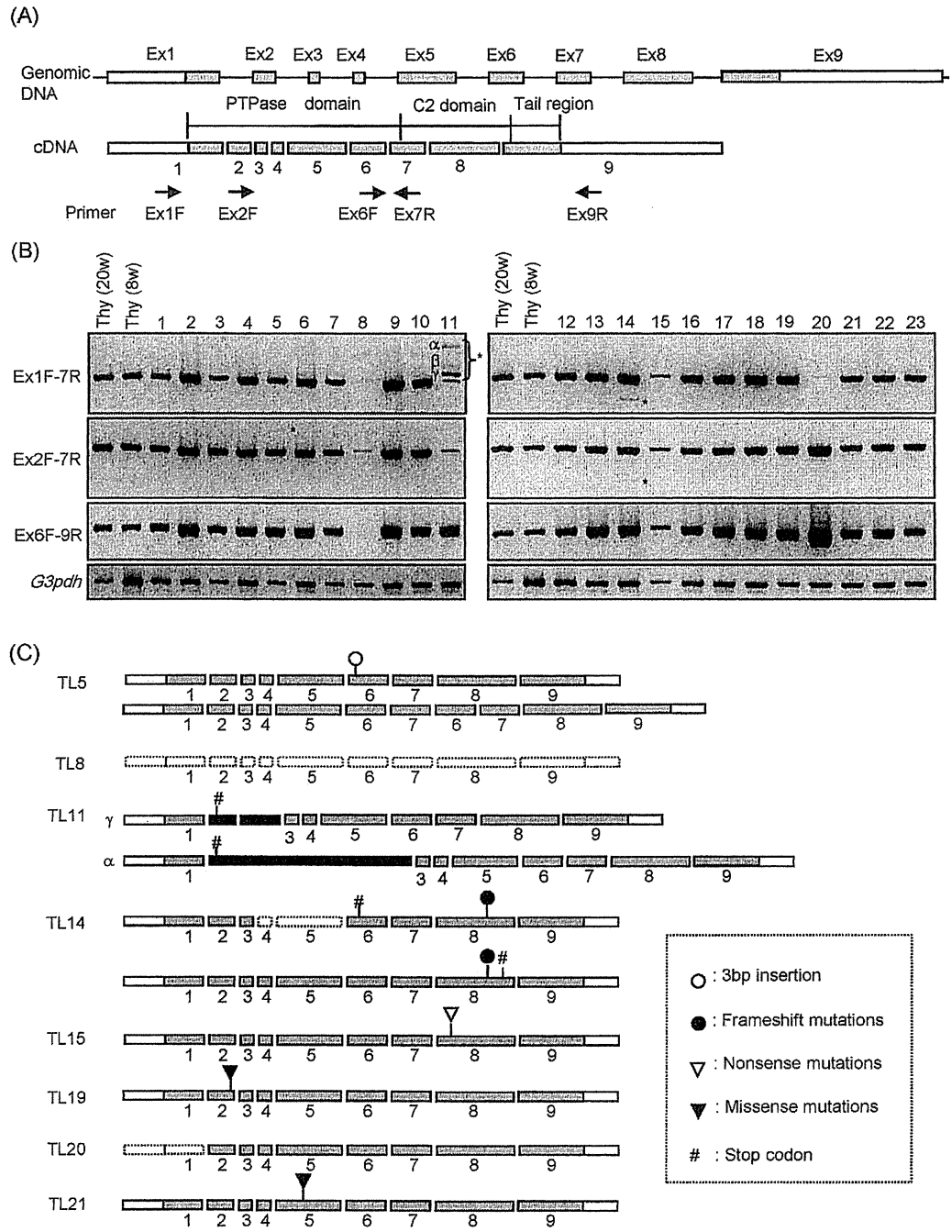

Fig. 2. Alteration of *Pten* in radiation-induced thymic lymphomas. (A) Schematic representation of *Pten*. Shading indicates the *Pten* coding regions. RT-PCR amplification primers and their annealing locations are indicated by arrows. Ex, exon; PTPase, phosphotyrosine protein phosphatase. (B) RT-PCR analysis of *Pten* using the primer pairs indicated at left and genomic DNA isolated from thymocytes (Thy) of 20- or 8-week-old mice (control lanes 1 and 2, respectively), or from the lymphoma indicated at top, was performed and reaction products were subjected to 2% agarose gel electrophoresis. *G3pdh* was used as a control for RT-PCR amplification and as a loading control. Asterisks indicate RT-PCR products longer or shorter than the expected size. (C) Schematic representation of aberrant *Pten* transcripts. Black bars in TL11 indicate inserted intronic sequences. #, Positions of newly generated in-frame stop codons that possibly cause immature translation.

terns in the 5′ (upstream) region of *Pten* (Supplementary Fig. 1A, indicated as P1) in all lymphomas; this region corresponds to the promoter of human *PTEN* that was shown to be aberrantly methylated in T-cell ALLs [26]. However, no aberrant methylation was detected (Supplementary Fig. 1B). Although the CpG sites at positions -39 and -40 relative to the transcriptional start site were both methylated in most of the lymphomas, these CpG sites were also frequently methylated in normal thymocytes. For TL8, we analyzed an additional *Pten* region (Supplementary Fig. 1A, indicated as P2) in which hypermethylation has been suggested to be associated with a lack of *PTEN* expression in non-small cell lung cancer [27]. However, we again did not detect aberrant methylation (Supplementary Fig. 1C). Thus, the absence of *Pten* transcripts likely resulted from a mechanism other than silencing by DNA methylation.

3.4. Sequence analysis of Pten transcripts

Next, we determined the sequence of the RT-PCR products from all lymphomas including those products that were longer or shorter than predicted in TL5, 11 and 14 (Fig. 2C). In TL5, the longer

PCR product generated using the Ex2F-7R primer pair contained duplicated exons 6 and 7. The product of predicted length had an insertion of 3 bp, which encoded an amino acid change from Ser170 to Met and Cys. Because the normal *Pten* sequence was not observed, TL5 may contain biallelic *Pten* mutations. TL11 had one RT-PCR product of predicted length and three longer products when amplified using the Ex1F-7R primer pair. The most predominant longer fragment generated from TL11 (Fig. 2B, indicated as γ) contained two large nucleotide insertions of 88 and 122 bp within intron 1 that generated a stop codon, together with a deletion of exon 2. The least predominant longer fragment generated from TL11 (Fig. 2B, indicated as α) contained a 1078-bp insertion in intron 1 and a deletion of exon 2, generating a stop codon. Sequencing of the TL11 PCR product β could not be achieved. The faint product of predicted length had no mutations but may have been derived from contamination of the tumor sample with healthy cells. In TL14, the predominant product of predicted length generated using the Ex6F-9R primer pair had a frameshift mutation due to a 1-bp insertion (962insA) in the poly(A)6 stretch in exon 8, creating a downstream stop codon. The faint/short PCR product of TL14, generated using either Ex1F-7R or Ex2F-7R primer pairs, had both the frameshift mutation and loss of exons 4 and 5, the latter of which generated a stop codon at residue 264. TL15 had an allele with a *Pten* nonsense mutation owing to a substitution (base 862G to T) in addition to a wild-type allele. TL19 had a *Pten* missense mutation owing to a substitution (base 158T to C), resulting in V53A. TL19 generated both mutated and wild-type PCR products, coincident with incomplete allelic LOH in TL19 (Fig. 1A). TL20 expressed only a single *Pten* transcript that lacked exon 1. TL21 had a missense mutation (base 364A to T) in *Pten*, resulting in I122F.

Overall, *Pten* transcripts in radiation-induced lymphomas had a variety of genetic lesions including missense mutations (TL19 and 21), nonsense mutations (TL15), 1- and 3-base insertions (TL14 and 5, respectively), partial intron insertions (TL11), exon duplication (TL5), exon deletion (TL11, 14, 20), and null expression (TL8). Although these mutations are very complicated, they were in good agreement with previous reports demonstrating that missense mutations occur in the Pten phosphatase domain whereas nonsense and frameshift mutations, resulting in protein truncation, occur in the C2 domain of Pten. In total, seven of eight lymphomas carrying a *Pten* mutation (88%) contained biallelic alterations.

3.5. Array-based comparative genomic hybridization (array-CGH) analysis of genomic DNA from TL8, 11 and 20

In order to know the reason for the absence or aberrant transcription of *Pten* in TL8, 11 and 20 (Fig. 2), we analyzed genomic structures around the *Pten* locus in TL8, 11 and 20 using array-CGH, which was designed for intensive analysis of the *Pten* locus. As shown in Fig. 3, the array-CGH profiles suggested partial homozygous deletions (<30 kbp) in the *Pten* locus in these lymphomas, which were positioned within the regions of hemizygous deletion in TL8 and 11. A region of homozygous deletion (~24 kbp) in TL8 occurred in the 5′ (upstream) region of *Pten*, encompassing both the putative promoter region and the transcription initiation site; this may account for the *Pten* silencing observed in TL8 (Fig. 2). Two RT-PCR products from TL11 had a deletion of exon 2 together with one or two insertion(s) of a partial sequence of intron 1 (Supplementary Fig. 2). Array-CGH indicated that TL11 had a homozygous deletion that extended 1 kbp downstream of exon 1 into the 5′ flanking region of exon 2, suggesting that the abnormal transcripts were generated by aberrant splice-site selection likely resulting from the absence of correct splice sites at the intron 1/exon 2 boundary. Array-CGH analysis of TL20 also revealed homozygous deletion of genomic regions (~4 kbp), including both the putative promoter region and the *Pten* transcription initiation site. RT-PCR analysis

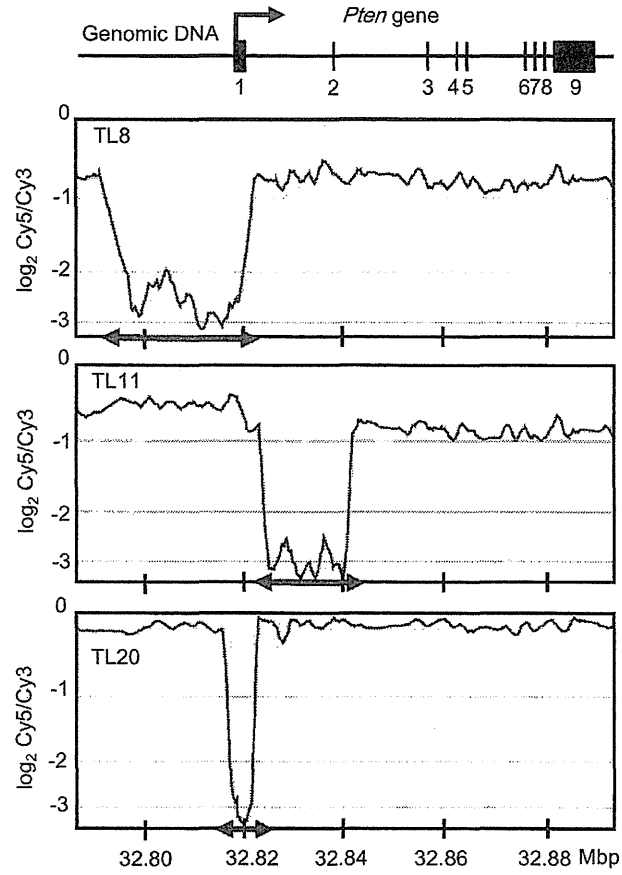

Fig. 3. Array-CGH analysis reveals homozygous focal deletions in three radiation-induced thymic lymphomas (TL8, 11 and 20). Schematic of *Pten* (top), in which shaded bars represent exons aligned to the genomic positions on chromosome 19 indicated along the *x*-axis in the array-CGH profiles below the schematic. Moving averages of the normalized $\log_2$ Cy5/Cy3 ratio, calculated based on 10 data points, are plotted in the array-CGH profiles. Arrows on the *x*-axis correspond to genomic regions amplified by PCR and sequenced to identify breakpoints.

indicated the presence of a *Pten* transcript, however, suggesting that the ectopic transcription was initiated at a cryptic promoter in TL20.

To explore the mechanism responsible for these deletions, genomic regions containing the breakpoints (indicated by the *x*-axis arrows in Fig. 3) were amplified by PCR and sequenced (Fig. 4), which identified nucleotide insertions at the breakpoint junctions in TL8 and 11. In TL11, a pair of recombination signal sequence-like sequences, composed of heptamer- and nonamer-like motifs separated by non-conserved spacers of 12 or 23 bp, were located between but immediately adjacent to the breakpoints, suggesting that illegitimate V(D)J recombination gave rise to the deletion. In contrast, a 0.8-kb templated nucleotide sequence was inserted in the TL20 deletion region. Overlaps of 1 or 2 nucleotides at both breakpoints of the two junctions were identified, suggesting that microhomology-mediated rearrangements might have led to the deletion.

3.6. Loss of Pten and downstream activation of Akt

Pten protein expression varied in the lymphomas we examined (Fig. 5). To determine whether decreased expression correlated with loss of Pten function, we analyzed the degree of Ser473 phosphorylation in Akt (Fig. 5). Pten was not expressed in lymphomas TL8, 11, 14 and 20, consistent with the aberrant stop codon and genomic deletions in the *Pten* promoter region. Pten expression level correlated inversely with phosphorylation of Akt. Lymphomas

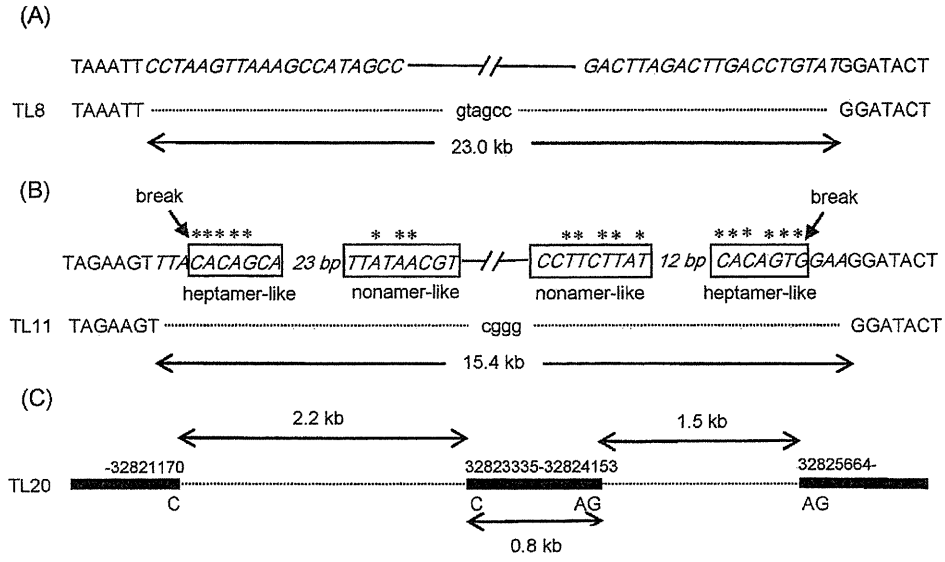

Fig. 4. Sequence analysis of *Pten* focal deletion breakpoints. Schematic diagram representing sequence analysis of focal deletion breakpoints in *Pten* in TL8 (A), TL11 (B) and TL20 (C) lymphomas. Dotted lines indicate deleted genomic regions, and the deleted wild-type sequence is shown in italics in (A and B). Boxes indicate heptamer-like or nonamer-like motifs, and nucleotides marked with asterisks are identical to the canonical heptamer or nonamer sequences. Arrows indicate the sites of Rag-mediated DNA breakage. Lowercase letters indicate nucleotide insertions. Black bars indicate the positions (mm8 assembly) of the retained DNA ends. The uppercase letters below the line in (C) indicate the sequences used to locate microhomology at both ends of each deletion.

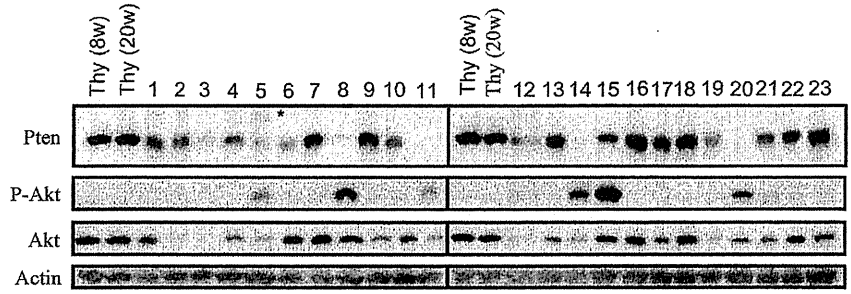

Fig. 5. Analysis of Pten expression and Akt phosphorylation in radiation-induced thymic lymphomas. Western blot analysis of lysates from 23 radiation-induced T-cell lymphomas was performed using antibodies to the proteins indicated at left. Lanes 1 and 2, control thymocytes (Thy) of 8- and 20-week-old mice, respectively. Actin was analyzed as loading control. Asterisk indicates polypeptide with larger mass than expected.

TL5, 19 and 21 expressed mutant Pten containing amino acid substitutions in the phosphatase domain. In TL5 and 21, Akt phosphorylation was weakly observed, suggesting dysfunction of Pten. In TL19, Akt phosphorylation was not observed. The lack of phosphorylation of Akt might have resulted from decreased levels of Akt protein. In TL3 and 12, in which the Pten expression level was low, Akt phosphorylation was not observed owing to negligible expression of Akt protein. In contrast, Akt was highly phosphorylated in TL15, which expressed wild-type Pten. It is possible that other factors that regulate the phosphorylation of Akt, such as PI3K and Ship, may activate Akt independently of Pten [28,29].

3.7. *Levels of Pten-targeting microRNAs do not correlate with Pten protein levels in lymphomas*

Lymphomas TL3, 6 and 12 contained low levels of Pten protein, although neither a decrease in the amounts of RT-PCR product nor genetic aberrations were observed. Recent reports have revealed the involvement of microRNAs in downregulation of Pten expression [13,14,30–33]. We therefore examined whether certain microRNAs contributed to post-transcriptional downregulation of the expression of Pten. For all lymphomas with sufficient available RNA, expression levels of the well-studied *Pten*-targeting microRNAs miR-19a and miR-21 were analyzed using real-time RT-PCR (Supplementary Fig. 3). Expression of miR-19a was almost constant among all lymphomas and was similar to the expression levels in normal thymocytes from 20-week-old mice. Some lymphomas exhibited relatively high miR-21 expression, but there was no significant inverse correlation between miR-21 expression level and Pten protein level.

4. Discussion

In our present study of radiation-induced thymic lymphomas, *Pten* inactivation occurred with a frequency of 30% (7 of 23 lymphomas) and was caused by a variety of biallelic structural abnormalities including base substitutions, long and short (1 and 3 bp) insertions, duplication, and deletions (Table 1). Epigenetic silencing was not observed.

Frequent LOH around the *PTEN* locus has been reported in human leukemias (20% frequency) and lymphomas (23% frequency) [34,35]. *PTEN* alterations, however, have only been sporadically detected in hematopoietic neoplasms [36–42]. In contrast, aberrant DNA methylation in the *PTEN* promoter region has been detected at a frequency of 20% in T-cell ALLs and at a frequency of 18% in B-cell ALLs [26], suggesting that epigenetic silencing is a dominant mechanism of *PTEN* inactivation in hematopoietic neoplasms. Santos et al. [22] has suggested that

Pten in radiation-induced mouse thymic lymphomas also undergoes epigenetic silencing in C57BL/6J and BALB/c F1 hybrid mice. In our present study, however, no aberrant DNA methylation was detected in CpG islands located in the 5′ (upstream) region of *Pten*. Thus, epigenetic silencing does not play a major role in *Pten* loss in radiation-induced thymic lymphomas in B6C3F1 mice. Mao et al. [61] also reported that *Pten* does not undergo methylation-mediated transcriptional silencing in $p53^{+/-}$and $p53^{-/-}$mice. The reason for these discrepancies is not clear, although different mice strains may exhibit distinct patterns of CpG island methylation. Indeed, it has been reported that patterns of CpG island methylation in T-cell lymphomas are driven by the genetic configuration of tumor cells [43]. Santos et al. [22] reported that intragenic mutations do not occur in any genes on chromosome 19, including *Pten*, in C57BL/6J and BALB/c F1 hybrid mice. In contrast, our data indicated frequent intragenic mutations of *Pten* in C57BL/6J and C3H/HeJ F1 hybrid mice, as was suggestive of the influence of the host genetic background on the mutation spectrum. We previously demonstrated strain-based differences between C57BL/6 and C3H mice with respect to genomic alterations of *Kras* and genome-wide copy numbers in thymic lymphomas [44,45].

We have shown that LOH of *Pten* occurred at a frequency of about 30% (7 of 23 lymphomas) and that 8 lymphomas contained complex *Pten* structural abnormalities. Most of the available information regarding the mutation spectrum of *PTEN* has been derived mainly from epithelial cancers such as endometrial carcinomas, glioblastomas, prostate carcinomas, and others [6,7]. In these cases missense, nonsense and frameshift mutations predominate; missense mutations have been found to cluster in exons 5 and 6, encoding the PTEN phosphatase domain, and nonsense and frameshift mutations cluster in the poly $(A)_6$ stretches and in exons 7 and 8, encoding the C2 domain [6]. Comparison of mutations has shown that *PTEN* mutations in tumors depend on tissue type. Endometrial carcinomas predominantly contain frameshift mutations (>60% frequency), whereas glioblastomas contain fewer frameshift mutations but more missense mutations (61% frequency). Recently, *PTEN* frameshift mutations were found to cluster exclusively in exon 7 in human T-cell ALLs [29]. On the other hand, hemizygous *PTEN* deletions have been reported in 39% of prostatic adenocarcinomas, and homozygous *PTEN* deletion has been observed in 5% of prostate tumors [46]. Of note, hemizygous *PTEN* deletion is usually accompanied by an interstitial microdeletion.

In this study, we detected focal homozygous deletions at *Pten* in 13% of lymphomas (3/23; TL8, 11 and 20), all of which resulted in dearth of Pten protein. In two lymphomas (TL8 and 11), homozygous deletions were positioned within hemizygous deletions, possibly resulting from independent deletions occurring in both alleles in these lymphomas. On the other hand, TL20 had a homozygous deletion without adjacent hemizygous deletions. The observation that TL20 contained distally extending continuous LOH on chromosome 19 suggests that this homozygous deletion might have been caused by sequential events, in which one small deletion within the *Pten* locus was followed by subsequent mitotic recombination. Notably, microdeletions have been reported in several key tumor-related genes, such as *IKZF1*, *PAX5* and *CDKN2A*, in human ALLs [47–51] and in *Nocth1* and *Bcl11b* in murine thymic lymphomas [52,53]. The sequence at the deletion breakpoint strongly suggests that these deletions were generated by illegitimate V(D)J recombination and microhomology-mediated rearrangement [49,52–54]. Homozygous *PTEN* deletions were recently identified in 4% of human primary childhood T-cell ALLs [29].

A previous study on T-cell lymphomas developed in chromosomally unstable *Terc*-, *Atm*- and *Trp53*-null mice also reported frequent homozygous deletions at the *Pten* locus [39]. In addition, recent reports on breast cancers [55] and medulloblastomas [56] demonstrated that *Pten* was selectively targeted in a background of defective homologous recombination repair of DNA double-strand breaks (DSBs). Importantly, radiation is a genotoxic stress that increases the frequency of DSBs and stimulates V(D)J rearrangements at cryptic recombination signal sequences [57]. Therefore, radiation-induced DNA DSBs may facilitate hemi- and homozygous deletions of the *Pten* locus.

The two-hit model posits that both copies of a tumor suppressor gene must be inactivated before cancer can develop [58]. Some tumor suppressor genes, however, are inactivated solely by hemizygous loss, indicating the involvement of haploinsufficiency. Several lines of evidence suggest that *Pten* is such a haploinsufficient tumor suppressor gene, at least in epithelial cancers such as prostate cancer [59,60]. A study of radiation-induced lymphomas from *Trp53* heterozygous and/or null mice suggested that *Pten* is a haploinsufficient tumor suppressor gene and that *Pten* haploinsufficiency is a common characteristic of radiation-induced lymphoma development [61]. It is unclear whether *Pten* is inactivated in a bi- or mono-allelic manner in thymic lymphomas of wild-type mice. In the present study, biallelic *Pten* inactivation occurred in seven of eight lymphomas. Although complete loss of *Pten* resulted in increased phosphorylation of Akt, lymphomas with decreased *Pten* expression or monoallelic inactivation (TL15) did not always exhibit increased Akt phosphorylation. Together with the frequent biallelic point mutations and microdeletions observed at the *Pten* locus, these findings suggest that decreased *Pten* dosage alone is not sufficient for activation of the PI3K/Akt signaling pathway during radiation-induced lymphomagenesis. Manifestation of *Pten* haploinsufficiency may require other genetic or epigenetic aberrations. It has been suggested that in tumors of defined tissue origin and genetic background, *Pten* functions in a haploinsufficient manner, but that for others both alleles need to be inactivated [62].

Conflicts of interest

The authors declare that there are no conflicts of interest.

Acknowledgements

The authors thank Dr. K. Ariyoshi, Mr. Y. Kodama and Ms. Y. Nishimura for their valuable technical tutorship and discussion. We also express our gratitude to all laboratory members for their encouragement throughout this work, and to the Laboratory Animal Science Section in National Institute of Radiological Sciences for animal management. This work was supported by institutional funds from the National Institute of Radiological Sciences (Chiba, Japan). This work was also supported financially by a Grant-in-Aid from the Ministry of Education, Culture, Sports, Sciences, and Technology of Japan (to Y.S.) and by a grant from the Long-Range Research Initiative of the Japan Chemical Industry Association (to Y.S. and S.K.).

Appendix A. Supplementary data

Supplementary data associated with this article can be found, in the online version, at doi:10.1016/j.mrfmmm.2009.12.011.

References

[1] V. Stambolic, A. Suzuki, J.L. de la Pompa, G.M. Brothers, C. Mirtsos, T. Sasaki, J. Ruland, J.M. Penninger, D.P. Siderovski, T.W. Mak, Negative regulation of PKB/Akt-dependent cell survival by the tumor suppressor PTEN, Cell 95 (1998) 29–39.

[2] H. Sun, R. Lesche, D.M. Li, J. Liliental, H. Zhang, J. Gao, N. Gavrilova, B. Mueller, X. Liu, H. Wu, PTEN modulates cell cycle progression and cell survival by regulating phosphatidylinositol 3,4,5,-trisphosphate and Akt/protein kinase B signaling pathway, Proc. Natl. Acad. Sci. U.S.A. 96 (1999) 6199–6204.